

Secure Transmission with Large Numbers of Antennas and Finite Alphabet Inputs

Yongpeng Wu, *Senior Member, IEEE*, Jun-Bo Wang, *Member, IEEE*, Jue Wang, *Member, IEEE*
Robert Schober, *Fellow, IEEE*, and Chengshan Xiao, *Fellow, IEEE*

Abstract—In this paper, we investigate secure transmission over the large-scale multiple-antenna wiretap channel with finite alphabet inputs. First, we investigate the case where instantaneous channel state information (CSI) of the eavesdropper is known at the transmitter. We show analytically that a generalized singular value decomposition (GSVD) based design, which is optimal for Gaussian inputs, may exhibit a severe performance loss for finite alphabet inputs in the high signal-to-noise ratio (SNR) regime. In light of this, we propose a novel Per-Group-GSVD (PG-GSVD) design which can effectively compensate the performance loss caused by the GSVD design. More importantly, the computational complexity of the PG-GSVD design is by orders of magnitude lower than that of the existing design for finite alphabet inputs in [1] while the resulting performance loss is minimal. Then, we extend the PG-GSVD design to the case where only statistical CSI of the eavesdropper is available at the transmitter. Numerical results indicate that the proposed PG-GSVD design can be efficiently implemented in large-scale multiple-antenna systems and achieves significant performance gains compared to the GSVD design.

I. INTRODUCTION

Security is a critical issue for future 5G wireless networks. In today's systems, the security provisioning relies on bit-level cryptographic mechanisms and associated processing techniques at various stages of the data protocol stack. However, these solutions have severe drawbacks and many weaknesses of standardized protection mechanisms for public wireless networks are well known; although enhanced ciphering and authentication protocols exist, they impose severe constraints and high additional costs for the users of public wireless networks [2]. Therefore, new security approaches based on information theoretical considerations have been proposed and are collectively referred to as physical layer security [1]–[28].

Most existing work on physical layer security assumes that the input signals are Gaussian distributed. Although the Gaussian codebook has been proved to achieve the secrecy capacity

of the Gaussian wiretap channel [7], the signals employed in practical communication systems are non-Gaussian and are often drawn from discrete constellations [29]–[32]. For the multiple-input, multiple-output, multiple antenna eavesdropper (MIMOME) wiretap channel with perfect channel state information (CSI) of both the desired user and the eavesdropper at the transmitter, a generalized singular value decomposition (GSVD) based precoding design was proposed to decouple the corresponding wiretap channel into independent parallel subchannels [26]. Then, the optimal power allocation policy across these subchannels was obtained by an iterative algorithm. However, the simulation results in [1] revealed that for finite alphabet inputs, the GSVD design is suboptimal. In fact, the iterative algorithm in [1] can significantly improve the secrecy rate by directly optimizing the precoder matrix. Furthermore, for finite alphabet inputs, both the receiver and the eavesdropper may accurately decode a transmitted message if the transmit power is sufficiently high. Therefore, the optimal precoder may not exploit the maximum available transmit power to maximize the secrecy rate in the high signal-to-noise ratio (SNR) regime [1], [26], [27]. Instead, it may be beneficial for the transmitter to use some of the available transmit power to inject artificial noise (AN) to interfere the decoding process of the eavesdropper. It has been shown in [1], [27] that injection of AN improves the secrecy rate for scenarios where the transmitter has only statistical CSI of the eavesdropper. Very recently, for the case when imperfect CSI of the eavesdropper is available at the transmitter, a secure transmission scheme was proposed in [28] based on the joint design of the transmit precoder matrix to improve the achievable rate of the desired user and the AN generation scheme to degrade the achievable rate of the eavesdropper. However, the computational complexities of the algorithms in [1] and [28] scale exponentially with the number of transmit antennas. Therefore, the algorithms in [1], [28] become intractable even for a moderate number of transmit antennas (e.g., eight).

In this paper, we investigate the secure transmission design for the large-scale MIMOME wiretap channel with finite alphabet inputs. The contributions of our paper are summarized as follows:

- 1) For scenarios where the instantaneous CSI of the eavesdropper is available at the transmitter, we derive an upper bound on the secrecy rate for finite alphabet inputs in the high SNR regime when the GSVD design is employed. The derived expression shows that, when $N_t > N_1$, in the high SNR regime, the GSVD design will result in at

Part of this paper was submitted to IEEE Globecom 2017.

Y. Wu is with Institute for Communications Engineering, Technical University of Munich, Theresienstrasse 90, D-80333 Munich, Germany (Email: yongpeng.wu2016@gmail.com).

Y. Wu and R. Schober are with the Institute for Digital Communications, University Erlangen-Nürnberg, Cauerstrasse 7, D-91058 Erlangen, Germany (Email: yongpeng.wu@fau.de; robert.schober@fau.de).

J.-B. Wang is with the National Mobile Communications Research Laboratory, Southeast University, Nanjing, 210096, P. R. China (Email: jbwang@seu.edu.cn).

J. Wang is with School of Electronics and Information, Nantong University, Nantong, 226000, P. R. China (Email: wangjue@ntu.edu).

C. Xiao is with the Department of Electrical and Computer Engineering, Missouri University of Science and Technology, Rolla, MO 65409, USA (Email: xiaoc@mst.edu).

least $(N_t - N_1) \log M$ b/s/Hz rate loss compared to the maximal rate for the MIMOME wiretap channel, where N_t , N_1 , and M denote the number of transmit antennas, the rank of the intended receiver's channel, and the size of the input signal constellation set, respectively.

- 2) To tackle this issue, we propose a novel Per-Group-GSVD (PG-GSVD) design, which pairs different subchannels into different groups based on the GSVD structure. We prove that the proposed PG-GSVD design can eliminate the performance loss of the GSVD design with an order of magnitude lower computational complexity than the design in [1]. Accordingly, we propose an iterative algorithm based on the gradient descent method to optimize the secrecy rate.
- 3) For the scenarios where only statistical CSI of the eavesdropper is available at the transmitter, we derive an achievable ergodic secrecy rate expression by invoking an upper bound on the average mutual information in fading multiple-input, multiple-output (MIMO) channels with finite alphabet inputs. Based on this, we extend the PG-GSVD design to the case where the transmitter has only statistical CSI of the eavesdropper.
- 4) By exploiting the low rank property of the transmit correlation matrices of massive MIMO channels [22], [33], [34], we derive a condition that the proposed PG-GSVD design for statistical CSI of the eavesdropper should satisfy to achieve the maximal secrecy rate for the MIMOME wiretap channel with finite alphabet inputs in the high SNR regime. For the cases where this condition does not hold, we propose an AN generation scheme that can further increase the secrecy rate performance.
- 5) Simulation results illustrate that the proposed designs are well suited for large-scale MIMO wiretap channels and achieve substantially higher secrecy rates than the GSVD design while requiring a much lower computational complexity than the precoder design in [1].

Notation: Vectors are denoted by lower-case bold-face letters; matrices are denoted by upper-case bold-face letters. Superscripts $(\cdot)^T$, $(\cdot)^*$, and $(\cdot)^H$ stand for the matrix transpose, conjugate, and conjugate-transpose operations, respectively. We use $\text{tr}(\mathbf{A})$ and \mathbf{A}^{-1} to denote the trace and the inverse of matrix \mathbf{A} , respectively. \perp denotes the orthogonal complement of a subspace. $\text{diag}\{\mathbf{b}\}$ denotes a diagonal matrix with the elements of vector \mathbf{b} on its main diagonal. $\text{Diag}\{\mathbf{B}\}$ denotes a diagonal matrix containing in the main diagonal the diagonal elements of matrix \mathbf{B} . The $M \times M$ identity matrix is denoted by \mathbf{I}_M , and the all-zero $M \times N$ matrix and the all-zero $N \times 1$ vector are denoted by $\mathbf{0}$. The fields of complex numbers and real numbers are denoted by \mathbb{C} and \mathbb{R} , respectively. $E[\cdot]$ denotes statistical expectation. $[\mathbf{A}]_{mn}$ denotes the element in the m th row and n th column of matrix \mathbf{A} . $[\mathbf{a}]_m$ denotes the m th entry of vector \mathbf{a} . We use $\mathbf{x} \sim \mathcal{CN}(\mathbf{0}, \mathbf{R}_N)$ to denote a circularly symmetric complex Gaussian vector $\mathbf{x} \in \mathbb{C}^{N \times 1}$ with zero mean and covariance matrix \mathbf{R}_N . $\text{null}(\mathbf{A})$ denotes the null space of matrix \mathbf{A} . \mathbf{e}_i denotes the unit-vector with a one as the i th element and zeros for all other elements.

II. SYSTEM MODEL

We study the MIMOME wiretap channel with a multiple-antenna transmitter (Alice), a multiple-antenna intended receiver (Bob), and a multiple-antenna eavesdropper (Eve), where the corresponding numbers of antennas are denoted by N_t , N_r , and N_e , respectively. The signals received at Bob and Eve are denoted by \mathbf{y}_b and \mathbf{y}_e , respectively, and can be written as

$$\mathbf{y}_b = \mathbf{H}_{ba} \mathbf{G} \mathbf{x}_a + \mathbf{n}_b \quad (1)$$

$$\mathbf{y}_e = \mathbf{H}_{ea} \mathbf{G} \mathbf{x}_a + \mathbf{n}_e \quad (2)$$

where $\mathbf{x}_a = [x_1, x_2, \dots, x_{N_t}]^T \in \mathbb{C}^{N_t \times 1}$ denotes the transmitted signal vector having zero mean and the identity matrix as covariance matrix, and $\mathbf{H}_{ba} \in \mathbb{C}^{N_r \times N_t}$ and $\mathbf{H}_{ea} \in \mathbb{C}^{N_e \times N_t}$ denote the channel matrices between Alice and Bob and between Alice and Eve, respectively. The complex independent identically distributed (i.i.d.) vectors $\mathbf{n}_b \sim \mathcal{CN}(0, \sigma_b^2 \mathbf{I}_{N_r})$ and $\mathbf{n}_e \sim \mathcal{CN}(0, \sigma_e^2 \mathbf{I}_{N_e})$ represent the channel noises at Bob and Eve, respectively. $\mathbf{G} \in \mathbb{C}^{N_t \times N_t}$ is a linear precoding matrix that has to be optimized for maximization of the secrecy rate. The precoding matrix has to satisfy the power constraint

$$\text{tr}\{E[\mathbf{G} \mathbf{x}_a \mathbf{x}_a^H \mathbf{G}^H]\} = \text{tr}\{\mathbf{G} \mathbf{G}^H\} \leq P. \quad (3)$$

In this paper, we assume that the transmitter has perfect instantaneous CSI of the intended receiver. For the eavesdropper's CSI available at the transmitter, we consider the following two cases:

- 1) The perfect instantaneous CSI of the eavesdropper is available at the transmitter. When the transmitter has perfect instantaneous knowledge of the eavesdropper's channel, the achievable secrecy rate is given by [7]

$$C_{\text{sec}} = \max_{\text{tr}(\mathbf{G} \mathbf{G}^H) \leq P} R_{\text{sec}}(\mathbf{G}) \quad (4)$$

$$R_{\text{sec}}(\mathbf{G}) = I(\mathbf{y}_b; \mathbf{x}_a) - I(\mathbf{y}_e; \mathbf{x}_a) \quad (5)$$

where $I(\mathbf{y}; \mathbf{x})$ denotes the mutual information between input \mathbf{x} and output \mathbf{y} .

- 2) Only statistical CSI of the eavesdropper is available at the transmitter. To ensure the consistency of the channel models for Bob and Eve, we assume that both \mathbf{H}_{ba} and \mathbf{H}_{ea} are Kronecker fading MIMO channels, i.e.,

$$\mathbf{H}_{ba} = \tilde{\mathbf{R}}_{N_b}^{1/2} \mathbf{H}_c \tilde{\mathbf{R}}_{N_t}^{1/2} \quad (6)$$

$$\mathbf{H}_{ea} = \mathbf{R}_{N_e}^{1/2} \mathbf{H}_w \mathbf{R}_{N_t}^{1/2} \quad (7)$$

where $\mathbf{H}_c \in \mathbb{C}^{N_r \times N_t}$ and $\mathbf{H}_w \in \mathbb{C}^{N_e \times N_t}$ are complex random matrices with independent random entries, which are distributed as $\mathcal{CN}(0, 1)$. Matrices $\tilde{\mathbf{R}}_{N_t} \in \mathbb{C}^{N_t \times N_t}$ and $\tilde{\mathbf{R}}_{N_b} \in \mathbb{C}^{N_b \times N_b}$ denote the transmit and receive correlation matrices of the intended receiver, respectively, whereas matrices $\mathbf{R}_{N_t} \in \mathbb{C}^{N_t \times N_t}$ and $\mathbf{R}_{N_e} \in \mathbb{C}^{N_e \times N_e}$ denote the transmit and receive correlation matrices of the eavesdropper, respectively. When the transmitter has only statistical CSI of Eve's channel, the achievable ergodic secrecy rate is given by [22]

$$\bar{C}_{\text{sec}} = \max_{\text{tr}(\mathbf{G} \mathbf{G}^H) \leq P} \bar{R}_{\text{sec}}(\mathbf{G}) \quad (8)$$

$$\bar{R}_{\text{sec}}(\mathbf{G}) = I(\mathbf{y}_b; \mathbf{x}_a) - E[I(\mathbf{y}_e; \mathbf{x}_a)]. \quad (9)$$

In this paper, we assume that perfect instantaneous CSI of the intended receiver is available at the transmitter [1], [6], [7], [9], [10], [21], [26], [27]. This assumption applies for scenarios where the intended receiver is static or the mobility of the intended receiver is low. In this case, the coherence time of the intended receiver's instantaneous channel is large. Therefore, the instantaneous CSI can be estimated accurately at the receiver based on training sequences and then be sent back to the transmitter through dedicated feedback links. In time division duplex systems, the instantaneous CSI can alternatively be obtained by exploiting the reciprocity of uplink and downlink.

For the eavesdropper, we consider two cases. The first case is that the eavesdropper is an idle user of the system and the transmitter intends to send a private message to a particular user of the system while regarding the other users as eavesdroppers. In this case, we assume perfect instantaneous CSI of eavesdropper can be obtained at the transmitter [6], [7], [9], [10], [21]. The second case is that the eavesdropper is always passive and does not transmit. In this case, we assume that only statistical CSI of the eavesdropper is available at the transmitter [4], [8], [11], [22].

The goal of this paper is to optimize the transmit precoding matrix \mathbf{G} for maximization of the secrecy rate in (5) or (9) when the transmit symbols \mathbf{x}_a are drawn from a discrete constellation set with M equiprobable points such as M -ary quadrature amplitude modulation (QAM) and N_t is large.

III. LOW COMPLEXITY PRECODER DESIGN WITH INSTANTANEOUS CSI OF THE EAVESDROPPER

In this section, we first provide some useful definitions which will be used in the subsequent analysis. Then, we analyze the rate loss of the GSVD design [26] compared to the maximal rate for finite alphabet inputs in the high SNR regime. Finally, we propose a PG-GSVD precoder to compensate this performance loss with low complexity.

A. Some Useful Definitions

Let us introduce some useful definitions for the subsequent analysis.

Definition 1: Similar to [7], [26], we define the following subspaces

$$\begin{aligned} \mathcal{S}_{ba} &= \text{null}(\mathbf{H}_{ba})^\perp \cap \text{null}(\mathbf{H}_{ea}) \\ \mathcal{S}_{be} &= \text{null}(\mathbf{H}_{ba})^\perp \cap \text{null}(\mathbf{H}_{ea})^\perp \\ \mathcal{S}_{ea} &= \text{null}(\mathbf{H}_{ba}) \cap \text{null}(\mathbf{H}_{ea})^\perp \\ \mathcal{S}_n &= \text{null}(\mathbf{H}_{ba}) \cap \text{null}(\mathbf{H}_{ea}). \end{aligned}$$

Define $k = \text{rank} \left(\begin{bmatrix} \mathbf{H}_{ba}^H & \mathbf{H}_{ea}^H \end{bmatrix}^H \right)$ and hence $\dim(\mathcal{S}_n) = N_t - k$. In addition, define $r = \dim(\mathcal{S}_{ba})$ and $s = \dim(\mathcal{S}_{be})$. Therefore, $\dim(\mathcal{S}_{ea}) = k - r - s$.

Definition 2: Following [7], we define the GSVD of the pair $(\mathbf{H}_{ba}, \mathbf{H}_{ea})$ as follows:

$$\mathbf{H}_{ba} = \mathbf{U}_{ba} \boldsymbol{\Sigma}_{ba} \begin{bmatrix} \boldsymbol{\Omega}^{-1} & \mathbf{0} \end{bmatrix} \mathbf{U}_a^H \quad (10)$$

$$\mathbf{H}_{ea} = \mathbf{U}_{ea} \boldsymbol{\Sigma}_{ea} \begin{bmatrix} \boldsymbol{\Omega}^{-1} & \mathbf{0} \end{bmatrix} \mathbf{U}_a^H \quad (11)$$

where $\mathbf{U}_a \in \mathbb{C}^{N_t \times N_t}$, $\mathbf{U}_{ba} \in \mathbb{C}^{N_r \times N_r}$, and $\mathbf{U}_{ea} \in \mathbb{C}^{N_e \times N_e}$ are unitary matrices. $\boldsymbol{\Omega} \in \mathbb{C}^{k \times k}$ is a non-singular matrix with diagonal elements ω_i , $i = 1, \dots, k$. $\boldsymbol{\Sigma}_{ba} \in \mathbb{C}^{N_r \times k}$ and $\boldsymbol{\Sigma}_{ea} \in \mathbb{C}^{N_e \times k}$ can be expressed as

$$\boldsymbol{\Sigma}_{ba} = \begin{matrix} & \begin{matrix} k-r-s & s & r \end{matrix} \\ \begin{matrix} N_r-r-s \\ s \\ r \end{matrix} & \begin{bmatrix} \mathbf{0} & \mathbf{0} & \mathbf{0} \\ \mathbf{0} & \mathbf{D}_b & \mathbf{0} \\ \mathbf{0} & \mathbf{0} & \mathbf{I}_r \end{bmatrix} \end{matrix} \quad (12)$$

$$\boldsymbol{\Sigma}_{ea} = \begin{matrix} & \begin{matrix} k-r-s & s & r \end{matrix} \\ \begin{matrix} k-r-s \\ s \\ N_e-k+r \end{matrix} & \begin{bmatrix} \mathbf{I}_{k-r-s} & \mathbf{0} & \mathbf{0} \\ \mathbf{0} & \mathbf{D}_e & \mathbf{0} \\ \mathbf{0} & \mathbf{0} & \mathbf{0} \end{bmatrix} \end{matrix} \quad (13)$$

where $\mathbf{D}_b = \text{diag}([b_1, \dots, b_s]) \in \mathbb{R}^{s \times s}$ and $\mathbf{D}_e = \text{diag}([e_1, \dots, e_s]) \in \mathbb{R}^{s \times s}$ are diagonal matrices with real valued entries. The diagonal elements of \mathbf{D}_b and \mathbf{D}_e are ordered as follows:

$$\begin{aligned} 0 < b_1 \leq b_2 \leq \dots \leq b_s < 1 \\ 1 > e_1 \geq e_2 \geq \dots \geq e_s > 0 \end{aligned}$$

and

$$b_p^2 + e_p^2 = 1, \text{ for } p = 1, \dots, s.$$

B. Performance Loss of the GSVD Design

The precoding matrix for the GSVD design can be expressed as [26]

$$\mathbf{G} = \mathbf{U}_a \mathbf{A} \mathbf{P}^{\frac{1}{2}} \quad (14)$$

where $\mathbf{P} = \text{diag}(p_1, \dots, p_{N_t})$ represents a diagonal power allocation matrix and \mathbf{A} is given by

$$\mathbf{A} = \begin{matrix} & \begin{matrix} k & N_t-k \end{matrix} \\ \begin{matrix} k \\ N_t-k \end{matrix} & \begin{bmatrix} \boldsymbol{\Omega} & \mathbf{0} \\ \mathbf{0} & \mathbf{0} \end{bmatrix} \end{matrix} \quad (15)$$

For the GSVD precoder design in (14), the received signals \mathbf{y}_b and \mathbf{y}_e in (1) and (2) can be re-expressed as

$$\tilde{\mathbf{y}}_b = \boldsymbol{\Sigma}_{ba} \begin{bmatrix} \mathbf{I}_k & \mathbf{0} \end{bmatrix} \mathbf{P}^{\frac{1}{2}} \mathbf{x}_a + \tilde{\mathbf{n}}_b \quad (16)$$

$$\tilde{\mathbf{y}}_e = \boldsymbol{\Sigma}_{ea} \begin{bmatrix} \mathbf{I}_k & \mathbf{0} \end{bmatrix} \mathbf{P}^{\frac{1}{2}} \mathbf{x}_a + \tilde{\mathbf{n}}_e \quad (17)$$

where $\tilde{\mathbf{y}}_b = \mathbf{U}_{ba}^H \mathbf{y}_b$, $\tilde{\mathbf{y}}_e = \mathbf{U}_{ea}^H \mathbf{y}_e$, $\tilde{\mathbf{n}}_b = \mathbf{U}_{ba}^H \mathbf{n}_b$, and $\tilde{\mathbf{n}}_e = \mathbf{U}_{ea}^H \mathbf{n}_e$.

Define $N_1 = \text{rank}(\mathbf{H}_{ba})$ and $N_2 = \text{rank}(\mathbf{H}_{ea})$. In the following theorem, we analyze the performance of the GSVD design for finite alphabet inputs in the high SNR regime.

Theorem 1: In the high SNR regime ($P \rightarrow \infty$), for the GSVD design in (14), the achievable secrecy rate $R_{\text{sec,high}}$ for finite alphabet signals is upper bounded by

$$R_{\text{sec,high}} \leq N_1 \log_2 M \text{ b/s/Hz}. \quad (18)$$

Proof: See Appendix A. \square

Theorem 1 indicates that the GSVD design may result in a severe performance loss for finite alphabet inputs in the high

SNR regime. For example, if $N_t > N_r$, which is a typical scenario for large-scale MIMO systems [35], [36], the GSVD design will cause a rate loss of at least $(N_t - N_r) \log_2 M$ b/s/Hz compared to the maximal rate in the high SNR regime. The precoder design in [1] avoids this performance loss by directly optimizing the precoder matrix \mathbf{G} . However, this results in an intractable implementation complexity for large-scale MIMO systems. Inspired by the idea of decoupling and grouping of point-to-point MIMO channels for finite alphabet inputs [37]–[39], we propose a PG-GSVD precoder design that prevents the performance loss of the GSVD design while retaining a low complexity in large-scale MIMOME channels.

C. PG-GSVD Precoder Design

As indicated in [39], in order to decouple the MIMO channels into N_t parallel subchannels, the MIMO channel matrix has to be an $N_t \times N_t$ matrix. However, Σ_{ba} and Σ_{ea} in (16) and (17) are $N_r \times N_t$ and $N_e \times N_t$ matrices, respectively. As a result, we need to add to or remove from $\tilde{\mathbf{y}}_b$, Σ_{ba} , $\tilde{\mathbf{y}}_e$, and Σ_{ea} some zeros in (16) and (17). To this end, we define

$$\tilde{\mathbf{y}}_b = \begin{matrix} k-r-s \\ r+s \\ N_t-k \end{matrix} \begin{bmatrix} \mathbf{0} \\ \tilde{\mathbf{y}}_b^H \\ \mathbf{0} \end{bmatrix}, \quad (19)$$

where $\tilde{\mathbf{y}}_b \in \mathbb{C}^{(r+s) \times 1}$ is composed of the last $r+s$ elements of $\tilde{\mathbf{y}}_b$. Furthermore, we define $\boldsymbol{\omega} = [\omega_1, \dots, \omega_k, \mathbf{0}^T]^H \in \mathbb{C}^{N_t \times 1}$, $\hat{\mathbf{y}}_e = [\tilde{\mathbf{y}}_e^H, \mathbf{0}^T]^H \in \mathbb{C}^{N_t \times 1}$, $\hat{\mathbf{n}}_b \sim \mathcal{CN}(0, \sigma_b^2 \mathbf{I}_{N_t})$, and $\hat{\mathbf{n}}_e \sim \mathcal{CN}(0, \sigma_e^2 \mathbf{I}_{N_t})$. Define two diagonal matrices

$$\hat{\Sigma}_{ba} = \begin{matrix} k-r-s & s & r & N_t-k \\ k-r-s & s & r & N_t-k \end{matrix} \begin{bmatrix} \mathbf{0} & \mathbf{0} & \mathbf{0} & \mathbf{0} \\ \mathbf{0} & \hat{\mathbf{D}}_b & \mathbf{0} & \mathbf{0} \\ \mathbf{0} & \mathbf{0} & \mathbf{R}_r & \mathbf{0} \\ \mathbf{0} & \mathbf{0} & \mathbf{0} & \mathbf{0} \end{bmatrix} \quad (20)$$

$$\hat{\Sigma}_{ea} = \begin{matrix} k-r-s & s & N_t-k+r \\ k-r-s & s & N_t-k+r \end{matrix} \begin{bmatrix} \mathbf{R}_{k-r-s} & \mathbf{0} & \mathbf{0} \\ \mathbf{0} & \hat{\mathbf{D}}_e & \mathbf{0} \\ \mathbf{0} & \mathbf{0} & \mathbf{0} \end{bmatrix} \quad (21)$$

where the elements of $\hat{\mathbf{D}}_b$, \mathbf{R}_r , \mathbf{R}_{k-r-s} , and $\hat{\mathbf{D}}_e$ are obtained from the following two equations

$$\left[\hat{\Sigma}_{ba} \right]_{(k-r-s+i)(k-r-s+i)} = \left[\Sigma_{ba} \right]_{(N_r-r-s+i)(k-r-s+i)} / \sqrt{\omega_i}, \quad i = 1, \dots, s+r \quad (22)$$

$$\left[\hat{\Sigma}_{ea} \right]_{ii} = \left[\Sigma_{ea} \right]_{ii} / \sqrt{\omega_i}, \quad i = 1, \dots, k-r. \quad (23)$$

We divide the transmit signal \mathbf{x}_a into S streams and let $N_s = N_t/S$ ¹. We define the set $\{\ell_1, \dots, \ell_{N_t}\}$ as a permutation of $\{1, \dots, N_t\}$. $\mathbf{P}_s \in \mathbb{C}^{N_s \times N_s}$ and $\mathbf{V}_s \in \mathbb{C}^{N_s \times N_s}$, $s = 1, \dots, S$, denote a diagonal and a unitary matrix, respectively. $\mathbf{V} \in$

$\mathbb{C}^{N_t \times N_t}$ denotes a unitary matrix. For the proposed PG-GSVD precoder, we set \mathbf{G} as follows

$$\mathbf{G} = \mathbf{U}_a \mathbf{A} \mathbf{P}^{\frac{1}{2}} \mathbf{V}. \quad (24)$$

We set

$$\left[\mathbf{P} \right]_{\ell_j \ell_j} = \left[\mathbf{P}_s \right]_{ii}, \quad (25)$$

where $i = 1, \dots, N_s$, $s = 1, \dots, S$, and $j = (s-1)N_s + i$.

Also, we set

$$\left[\mathbf{V} \right]_{\ell_i \ell_j} = \begin{cases} \left[\mathbf{V}_s \right]_{mn} & \text{if } i = (s-1)N_s + m, j = (s-1)N_s + n \\ 0 & \text{otherwise} \end{cases} \quad (26)$$

where $m = 1, \dots, N_s$, $n = 1, \dots, N_s$, $s = 1, \dots, S$, $i = 1, \dots, N_t$, and $j = 1, \dots, N_t$. Finally, we let

$$\left[\mathbf{x}_s \right]_i = \left[\mathbf{x}_a \right]_{\ell_j}. \quad (27)$$

Based on (24)–(27) and a pairing scheme $\{\ell_1, \dots, \ell_{N_t}\}$, the equivalent received signals at Bob and Eve can be decoupled as follows

$$\left[\hat{\mathbf{y}}_b \right]_{\ell_j} = \left[\hat{\Sigma}_{ba} \right]_{\ell_j \ell_j} \left[\hat{\mathbf{x}} \right]_{\ell_j} + \left[\hat{\mathbf{n}}_b \right]_{\ell_j} \quad (28)$$

$$\left[\hat{\mathbf{y}}_e \right]_{\ell_j} = \left[\hat{\Sigma}_{ea} \right]_{\ell_j \ell_j} \left[\hat{\mathbf{x}} \right]_{\ell_j} + \left[\hat{\mathbf{n}}_e \right]_{\ell_j} \quad (29)$$

where

$$\left[\hat{\mathbf{x}} \right]_{\ell_j} = \left[\mathbf{P}_s^{\frac{1}{2}} \mathbf{V}_s \mathbf{x}_s \right]_i \quad (30)$$

for $i = 1, \dots, N_s$, $s = 1, \dots, S$, and $j = (s-1)N_s + i$. From (28) and (29), we observe that the transmit signal has been divided into S independent groups. In each group, the equivalent signal dimension is $N_s \times 1$. We further define $\left[\hat{\mathbf{y}}_b \right]_{\ell_j} = \left[\mathbf{y}_{b,s} \right]_i$ and $\left[\hat{\mathbf{y}}_e \right]_{\ell_j} = \left[\mathbf{y}_{e,s} \right]_i$.

Based on (28) and (29), the secrecy rate in (5) can be expressed as

$$R_{\text{sec}}(\mathbf{G}) = \sum_{s=1}^S (I(\mathbf{y}_{b,s}; \mathbf{x}_s) - I(\mathbf{y}_{e,s}; \mathbf{x}_s)). \quad (31)$$

Algorithm 1: Maximizing $R_{\text{sec}}(\mathbf{G})$ with respect to \mathbf{P}_s and \mathbf{V}_s .

-
- 1) Initialize \mathbf{P}_s and $\mathbf{V}_s^{(0)}$ for $s = 1, \dots, S$ with $\text{tr}(\mathbf{A} \mathbf{P}_s^H) = N_t$. Set N_{iter} and ε as the maximum iteration number and a threshold, respectively.
 - 2) Initialize $R_{\text{sec}}(\mathbf{G})^{(1)}$ based on (31). Set counter $n = 1$.
 - 3) Update $\mathbf{P}_s^{(n)}$ for $s = 1, \dots, S$ along the gradient decent direction $\nabla_{\mathbf{P}_s} R(\mathbf{G})$.
 - 4) Normalize $\text{tr}(\mathbf{P}_s^{(n)})$ to satisfy $\text{tr}(\mathbf{A} \mathbf{P}_s^H) = N_t$.
 - 5) Update $\mathbf{V}_s^{(n)}$ for $s = 1, \dots, S$ along the gradient descent direction $\nabla_{\mathbf{V}_s} R(\mathbf{G})$.
 - 6) Compute $R_{\text{sec}}(\mathbf{G})^{(n+1)}$ based on (31). If $R_{\text{sec}}(\mathbf{G})^{(n+1)} - R_{\text{sec}}(\mathbf{G})^{(n)} > \varepsilon$ and $n \leq N_{\text{iter}}$, set $n = n + 1$ and repeat Steps 3–5;
 - 7) Compute \mathbf{P} and \mathbf{V} based on (25) and (26). Set $\mathbf{G} = \mathbf{U}_a \mathbf{A} \mathbf{P}^{\frac{1}{2}} \mathbf{V}$.
-

¹For convenience, we assume $N_s = N_t/S$ is an integer in this paper. If N_t/S is not an integer, we can easily obtain an integer N_s by adding zeros in (20) and (21).

The gradients of $I(\mathbf{y}_{b,s}; \mathbf{x}_s)$ and $I(\mathbf{y}_{e,s}; \mathbf{x}_s)$ with respect to \mathbf{P}_s and \mathbf{V}_s can be found in [40, Eq. (22)], based on which an iterative algorithm can be derived for maximizing $R_{\text{sec}}(\mathbf{G})$, as given in Algorithm 1.

Remark 1: For precoder design for the MIMO wiretap channel with finite alphabet inputs, the computational complexity is dominated [41] by the computation of the mutual information in [1, Eq. (12)] and [1, Eq. (13)]. We note that the expectations over the noise vector in [1, Eq. (12)] and [1, Eq. (13)] can be evaluated by an accurate approximation as in [41, Prop. 2]. Therefore, the corresponding computational complexities are negligible. Also, we note that computing the expectation over \mathbf{x}_a for the mutual information in [1, Eq. (12)] and [1, Eq. (13)] and the corresponding mean square error (MSE) matrix in [1, Eq. (17)] and [1, Eq. (18)] involves additions over the modulation signal space which scales exponentially with the number of transmit antennas. The computational complexities of other operations, such as the matrix product and the GSVD decomposition, are polynomial functions of the number of transmit and receive antennas. Therefore, for ease of analysis, we just consider the computational complexity of calculating the mutual information and the MSE matrix for comparing the complexities of Algorithm 1 and the complete-search design in [1]. For large N_t , the computational complexity of the complete-search design in [1] is dominated by number of additions needed for calculating the mutual information and the MSE matrix in [1, Eq. (12)], [1, Eq. (13)], [1, Eq. (17)], and [1, Eq. (18)]. Accordingly, the computational complexity of the complete-search design scales linearly with M^{2N_t} . In contrast, the computational complexity of calculating the mutual information and the MSE matrix in Algorithm 1 based on (31) and [40, Eq. (22)] grows linearly with SM^{2N_s} . As a result, the computational complexity of Algorithm 1 can be significantly lower than that of the complete-search design when the number of transmit antennas is large.

Remark 2: We note that Algorithm 1 never decreases the secrecy rate $R_{\text{sec}}(\mathbf{G})$ in any iteration, see Step 6. Also, for finite alphabet input signals, we know that the secrecy rate $R_{\text{sec}}(\mathbf{G})$ is upper-bounded. This indicates that Algorithm 1 generates a non-decreasing sequence which is upper-bounded. Therefore, Algorithm 1 is convergent. Due to the non-convexity of the objective function $R_{\text{sec}}(\mathbf{G})$, Algorithm 1 will reach a local optimal point of the secrecy rate in general. As a result, we implement Algorithm 1 for several random initializations for \mathbf{P}_s and \mathbf{V}_s and choose the result that achieves the highest secrecy rate as the final design solution [42], [43].

For the PG-GSVD design in (24), we have the following theorem.

Theorem 2: If the inequality $(k - N_2)N_s \geq N_t$ holds, then we can always find a permutation $\{\ell_1, \dots, \ell_{N_t}\}$ for the PG-GSVD design in (24), which achieves $R_{\text{sec,high}} = N_t \log_2 M$ b/s/Hz in the high SNR regime. *Proof:* See Appendix B. \square

The algorithm in [1] is equivalent to setting $N_s = N_t$ in Algorithm 1. Therefore, as long as $k - N_2 \neq 0$, it can compensate the performance loss of the GSVD design and achieve the saturation rate $N_t \log_2 M$ b/s/Hz in the high SNR

regime, as shown in [1, Figs. 1, 2]. However, in this case, the computational complexity of the algorithm in [1] grows exponentially with N_t . This is prohibitive in large-scale MIMO systems. For typical large-scale MIMO systems, we have $N_t > N_2$ [35], [36], which implies $k - N_2 \neq 0$. As a result, by properly choosing N_s , we can reach a favorable trade-off between complexity and secrecy rate performance².

To better illustrate the GSVD design, the precoder design in [1], and the PG-GSVD design, we provide the following example.

Example 1: We consider a MIMOME model with $N_t = 4$, $N_r = 3$, $N_e = 2$, and $N_s = 2$. Let $\mathbf{x}_a = [x_1, x_2, x_3, x_4]^T$. $[\hat{\mathbf{D}}_b]_{ii}$, $[\mathbf{R}_r]_{ii}$, $[\mathbf{R}_{k-r-s}]_{ii}$, and $[\hat{\mathbf{D}}_e]_{ii}$ in (20) and (21) are denoted as $D_{b,i}$, $R_{r,i}$, $R_{k-r-s,i}$, and $D_{e,i}$, respectively. $[\mathbf{V}]_{ij}$ is denoted as v_{ij} . Based on (20) and (21), the equivalent received signals $\hat{\mathbf{y}}_b$ and $\hat{\mathbf{y}}_e$ for the GSVD design are given by

$$\hat{\mathbf{y}}_b = \begin{bmatrix} 0 & 0 & 0 & 0 \\ 0 & D_{b,1} & 0 & 0 \\ 0 & 0 & R_{r,1} & 0 \\ 0 & 0 & 0 & R_{r,2} \end{bmatrix} \begin{bmatrix} p_1 & 0 & 0 & 0 \\ 0 & p_2 & 0 & 0 \\ 0 & 0 & p_3 & 0 \\ 0 & 0 & 0 & p_4 \end{bmatrix} \times \begin{bmatrix} x_1 \\ x_2 \\ x_3 \\ x_4 \end{bmatrix} + \hat{\mathbf{n}}_b \quad (32a)$$

$$= \begin{bmatrix} 0 \\ p_2 D_{b,1} x_2 \\ p_3 R_{r,1} x_3 \\ p_4 R_{r,2} x_4 \end{bmatrix} + \hat{\mathbf{n}}_b \quad (32b)$$

$$\hat{\mathbf{y}}_e = \begin{bmatrix} R_{k-r-s,1} & 0 & 0 & 0 \\ 0 & D_{e,1} & 0 & 0 \\ 0 & 0 & 0 & 0 \\ 0 & 0 & 0 & 0 \end{bmatrix} \begin{bmatrix} p_1 & 0 & 0 & 0 \\ 0 & p_2 & 0 & 0 \\ 0 & 0 & p_3 & 0 \\ 0 & 0 & 0 & p_4 \end{bmatrix} \times \begin{bmatrix} x_1 \\ x_2 \\ x_3 \\ x_4 \end{bmatrix} + \hat{\mathbf{n}}_e \quad (33a)$$

$$= \begin{bmatrix} p_1 R_{k-r-s,1} x_1 \\ p_2 D_{e,1} x_2 \\ 0 \\ 0 \end{bmatrix} + \hat{\mathbf{n}}_e. \quad (33b)$$

We observe from (32b) and (33b) that the GSVD design decouples the original MIMO wiretap channel into four parallel subchannels. In subchannel 3 and 4, x_3 and x_4 are received by Bob but not by Eve, respectively. In subchannel 1, x_1 is received by Eve but not by Bob. In subchannel 2, according to [26, Eq. (12)], if $D_{b,1} < D_{e,1}$, we set $p_2 = 0$. As a result, for the GSVD design, x_1 is definitely not received by Bob and x_2 may also not be received by Bob.

²We note that as long as $k - N_2 \neq 0$, the proposed PG-GSVD design can also be applied in cases where the transmitter is equipped with fewer antennas than the receiver.

The equivalent received signals $\hat{\mathbf{y}}_b$ and $\hat{\mathbf{y}}_e$ for the design in [1] are given by

$$\hat{\mathbf{y}}_b = \begin{bmatrix} 0 & 0 & 0 & 0 \\ 0 & D_{b,1} & 0 & 0 \\ 0 & 0 & R_{r,1} & 0 \\ 0 & 0 & 0 & R_{r,2} \end{bmatrix} \begin{bmatrix} p_1 & 0 & 0 & 0 \\ 0 & p_2 & 0 & 0 \\ 0 & 0 & p_3 & 0 \\ 0 & 0 & 0 & p_4 \end{bmatrix} \times \begin{bmatrix} v_{11} & v_{12} & v_{13} & v_{14} \\ v_{21} & v_{22} & v_{23} & v_{24} \\ v_{31} & v_{32} & v_{33} & v_{34} \\ v_{41} & v_{42} & v_{43} & v_{44} \end{bmatrix} \begin{bmatrix} x_1 \\ x_2 \\ x_3 \\ x_4 \end{bmatrix} + \hat{\mathbf{n}}_b \quad (34a)$$

$$= \begin{bmatrix} 0 \\ p_2 D_{b,1} \sum_{i=1}^4 v_{2i} x_i \\ p_3 R_{r,1} \sum_{i=1}^4 v_{3i} x_i \\ p_4 R_{r,2} \sum_{i=1}^4 v_{4i} x_i \end{bmatrix} + \hat{\mathbf{n}}_b \quad (34b)$$

$$\hat{\mathbf{y}}_e = \begin{bmatrix} R_{k-r-s,1} & 0 & 0 & 0 \\ 0 & D_{e,1} & 0 & 0 \\ 0 & 0 & 0 & 0 \\ 0 & 0 & 0 & 0 \end{bmatrix} \begin{bmatrix} p_1 & 0 & 0 & 0 \\ 0 & p_2 & 0 & 0 \\ 0 & 0 & p_3 & 0 \\ 0 & 0 & 0 & p_4 \end{bmatrix} \times \begin{bmatrix} v_{11} & v_{12} & v_{13} & v_{14} \\ v_{21} & v_{22} & v_{23} & v_{24} \\ v_{31} & v_{32} & v_{33} & v_{34} \\ v_{41} & v_{42} & v_{43} & v_{44} \end{bmatrix} \begin{bmatrix} x_1 \\ x_2 \\ x_3 \\ x_4 \end{bmatrix} + \hat{\mathbf{n}}_e \quad (35a)$$

$$= \begin{bmatrix} p_1 R_{k-r-s,1} \sum_{i=1}^4 v_{1i} x_i \\ p_2 D_{e,1} \sum_{i=1}^4 v_{2i} x_i \\ 0 \\ 0 \end{bmatrix} + \hat{\mathbf{n}}_e \quad (35b)$$

We observe from (34b) and (35b) that for the design in [1], by setting $p_1 = p_2 = 0$, x_1 , x_2 , x_3 , and x_4 are combined and transmitted along subchannel 3 and subchannel 4, which can be received by Bob but not by Eve. However, in this case, we need to calculate the expectation over (x_1, x_2, x_3, x_4) for evaluating the mutual information and the MSE matrix, which requires $4^{2 \times 4} = 65536$ additions for quadrature phase shift keying (QPSK) inputs.

The equivalent received signals $\hat{\mathbf{y}}_b$ and $\hat{\mathbf{y}}_e$ for the PG-GSVD design are given by

$$\hat{\mathbf{y}}_b = \begin{bmatrix} 0 & 0 & 0 & 0 \\ 0 & D_{b,1} & 0 & 0 \\ 0 & 0 & R_{r,1} & 0 \\ 0 & 0 & 0 & R_{r,2} \end{bmatrix} \begin{bmatrix} p_1 & 0 & 0 & 0 \\ 0 & p_2 & 0 & 0 \\ 0 & 0 & p_3 & 0 \\ 0 & 0 & 0 & p_4 \end{bmatrix} \times \begin{bmatrix} v_{11} & 0 & 0 & v_{14} \\ 0 & v_{22} & v_{23} & 0 \\ 0 & v_{32} & v_{33} & 0 \\ v_{41} & 0 & 0 & v_{44} \end{bmatrix} \begin{bmatrix} x_1 \\ x_2 \\ x_3 \\ x_4 \end{bmatrix} + \hat{\mathbf{n}}_b \quad (36a)$$

$$= \begin{bmatrix} 0 \\ p_2 D_{b,1} (v_{22} x_2 + v_{23} x_3) \\ p_3 R_{r,1} (v_{32} x_2 + v_{33} x_3) \\ p_4 R_{r,2} (v_{41} x_1 + v_{44} x_4) \end{bmatrix} + \hat{\mathbf{n}}_b \quad (36b)$$

$$\hat{\mathbf{y}}_e = \begin{bmatrix} R_{k-r-s,1} & 0 & 0 & 0 \\ 0 & D_{e,1} & 0 & 0 \\ 0 & 0 & 0 & 0 \\ 0 & 0 & 0 & 0 \end{bmatrix} \begin{bmatrix} p_1 & 0 & 0 & 0 \\ 0 & p_2 & 0 & 0 \\ 0 & 0 & p_3 & 0 \\ 0 & 0 & 0 & p_4 \end{bmatrix} \times \begin{bmatrix} v_{11} & 0 & 0 & v_{14} \\ 0 & v_{22} & v_{23} & 0 \\ 0 & v_{32} & v_{33} & 0 \\ v_{41} & 0 & 0 & v_{44} \end{bmatrix} \begin{bmatrix} x_1 \\ x_2 \\ x_3 \\ x_4 \end{bmatrix} + \hat{\mathbf{n}}_e \quad (37a)$$

$$= \begin{bmatrix} p_1 R_{k-r-s,1} (v_{11} x_1 + v_{14} x_4) \\ p_2 D_{e,1} (v_{22} x_2 + v_{23} x_3) \\ 0 \\ 0 \end{bmatrix} + \hat{\mathbf{n}}_e \quad (37b)$$

We observe from (36b) and (37b) that for the PG-GSVD design, x_1 and x_4 are combined and transmitted over subchannel 4. For x_2 , even if $D_{b,1} < D_{e,1}$, it can be combined with x_3 and transmitted over subchannel 3. For the PG-GSVD design, by setting $p_1 = p_2 = 0$, x_1 , x_2 , x_3 , and x_4 can also be received by Bob but not by Eve. As a result, the PG-GSVD design compensates the performance loss caused by the GSVD design. In this case, we only need to calculate the expectation over (x_1, x_4) and (x_2, x_3) for evaluating the mutual information and the MSE matrix, which requires $2 \times 4^{2 \times 2} = 512$ additions for QPSK inputs.

IV. LOW COMPLEXITY PRECODER DESIGN WITH STATISTICAL CSI OF EVE

If only statistical CSI of Eve is available at the transmitter, the PG-GSVD design in Section III-C can not be directly applied to maximize the ergodic secrecy rate in (9). This is because in (9), the expectation over all possible realizations of Eve's channel is needed. It is impossible to find a single precoder matrix to decouple all channel realizations simultaneously. However, by exploiting the asymptotic approximation results in [43], we can establish the deterministic equivalent channel of Eve, based on which the PG-GSVD design in Section III-C can be applied directly. However, this design has two major drawbacks. First, the iterative algorithm formulated based on this equivalent channel requires the calculation of the corresponding asymptotic parameters in each iteration (see Step 4 in Algorithm 1 in [43]), which increases the computational burden. More importantly, this equivalent channel is obtained under the assumption that N_t and N_e approach infinity simultaneously. However, whether this secrecy rate is achievable when the antenna dimensions are finite is unknown. In this section, we first propose a low complexity precoder design to maximize an achievable secrecy rate with statistical CSI of Eve. Then, we discuss the role of AN.

A. PG-GSVD Design with Statistical CSI

In this subsection, we derive a lower bound on (9), which is an achievable secrecy rate that does not depend on the instantaneous eavesdropper channel but only depends on the correlation matrices \mathbf{R}_{N_e} and \mathbf{R}_{N_t} . Then, we propose a precoder structure that decomposes these matrices into small

dimensions, which forms the basis for a low complexity precoder design.

Let $\mathbf{R}_{N_t} = \mathbf{T}^H \mathbf{T}$. Define the GSVD of the pair $(\mathbf{H}_{ba}, \mathbf{T})$ as follows:

$$\mathbf{H}_{ba} = \mathbf{U}_{ba,\text{erg}} \boldsymbol{\Sigma}_{ba,\text{erg}} \begin{bmatrix} k_{\text{erg}} & N_t - k_{\text{erg}} \\ \boldsymbol{\Omega}_{\text{erg}}^{-1} & \mathbf{0} \end{bmatrix} \mathbf{U}_{a,\text{erg}}^H \quad (38)$$

$$\mathbf{T} = \mathbf{U}_{ea,\text{erg}} \boldsymbol{\Sigma}_{ea,\text{erg}} \begin{bmatrix} k_{\text{erg}} & N_t - k_{\text{erg}} \\ \boldsymbol{\Omega}_{\text{erg}}^{-1} & \mathbf{0} \end{bmatrix} \mathbf{U}_{a,\text{erg}}^H \quad (39)$$

where $\mathbf{U}_{ba,\text{erg}}$, $\boldsymbol{\Sigma}_{ba,\text{erg}}$, $\mathbf{U}_{a,\text{erg}}$, $\mathbf{U}_{ea,\text{erg}}$, $\boldsymbol{\Sigma}_{ea,\text{erg}}$, \mathbf{A}_{erg} , $\boldsymbol{\Omega}_{\text{erg}}$, k_{erg} , r_{erg} , and s_{erg} are obtained by replacing \mathbf{H}_{ea} with \mathbf{T} in Section III-A.

Also, we define

$$\hat{\boldsymbol{\Sigma}}_{ea,\text{erg}} = \begin{matrix} k_{\text{erg}} - r_{\text{erg}} - s_{\text{erg}} & s_{\text{erg}} & N_t - k_{\text{erg}} + r_{\text{erg}} \\ \begin{bmatrix} \mathbf{R}_{\text{erg}} & \mathbf{0} & \mathbf{0} \\ \mathbf{0} & \hat{\mathbf{D}}_{e,\text{erg}} & \mathbf{0} \\ \mathbf{0} & \mathbf{0} & \mathbf{0} \end{bmatrix} \end{matrix} \quad (40)$$

where the elements of \mathbf{R}_{erg} and $\hat{\mathbf{D}}_{e,\text{erg}}$ are obtained from the following equation:

$$\left[\hat{\boldsymbol{\Sigma}}_{ea,\text{erg}} \right]_{ii} = \frac{[\boldsymbol{\Sigma}_{ea,\text{erg}}]_{ii}}{\sqrt{\omega_{i,\text{erg}}}}, \quad i = 1, \dots, k_{\text{erg}} - r_{\text{erg}} \quad (41)$$

where $\omega_{i,\text{erg}}$ is the i th diagonal element of $\boldsymbol{\Omega}_{\text{erg}}$. Let \mathbf{x}_q denote the q th element of the transmit signal constellation set and $\mathbf{b}_{pq} = \mathbf{x}_p - \mathbf{x}_q$, $p = 1, \dots, M^{N_t}$, $q = 1, \dots, M^{N_t}$. We further define $[\hat{\boldsymbol{\Sigma}}_{ea,\text{erg}}]_{\ell_j \ell_j} = [\hat{\boldsymbol{\Sigma}}_s]_{ii}$ and $[\mathbf{b}_{pq}]_{\ell_j \ell_j} = [\mathbf{b}_{s,pq}]_{ii}$ for $i = 1, \dots, N_s$, $s = 1, \dots, S$, and $j = (s-1)N_s + i$. $\mathbf{P}_{\text{erg}} \in \mathbb{C}^{N_t \times N_t}$ and $\mathbf{V}_{\text{erg}} \in \mathbb{C}^{N_t \times N_t}$ denote a diagonal and a unitary matrix, respectively. Replace \mathbf{P}_s , \mathbf{V}_s , \mathbf{P} , and \mathbf{V} in (25) and (26) with $\mathbf{P}_{s,\text{erg}} \in \mathbb{C}^{N_s \times N_s}$, $\mathbf{V}_{s,\text{erg}} \in \mathbb{C}^{N_s \times N_s}$, \mathbf{P}_{erg} , and \mathbf{V}_{erg} , respectively. Then, we have the following theorem.

Theorem 3: By setting $\mathbf{G}_{\text{erg}} = \mathbf{U}_{a,\text{erg}} \mathbf{A}_{\text{erg}} \mathbf{P}_{\text{erg}}^{\frac{1}{2}} \mathbf{V}_{\text{erg}}$, a lower bound on $\bar{R}_{\text{sec}}(\mathbf{G})$ in (9) is given by

$$\bar{R}_{\text{sec}}(\mathbf{G}) \geq \bar{R}_{\text{sec},1}(\mathbf{G}) = \sum_{s=1}^S I(\mathbf{y}_{b,s,\text{erg}}; \mathbf{x}_{s,\text{erg}}) - R_{\text{eve},u}, \quad (42)$$

where $\mathbf{y}_{b,s,\text{erg}}$ and $\mathbf{x}_{s,\text{erg}}$ are obtained by replacing \mathbf{H}_{ea} with \mathbf{T} in Section III-C and $R_{\text{eve},u}$ is given by

$$R_{\text{eve},u} = N_t \log M - \frac{1}{M^{N_t}} \sum_{s=1}^S \sum_{p_s=1}^{M^{N_s}} \log \sum_{q_s=1}^{M^{N_s}} \exp \left(-\frac{\text{tr}(\mathbf{R}_{N_e})}{\sigma_e^2} \right) \times \mathbf{b}_{s,p_s,q_s}^H \mathbf{V}_{s,\text{erg}}^H \mathbf{P}_{s,\text{erg}}^{\frac{1}{2}} \hat{\boldsymbol{\Sigma}}_s^2 \mathbf{P}_{s,\text{erg}}^{\frac{1}{2}} \mathbf{V}_{s,\text{erg}} \mathbf{b}_{s,p_s,q_s}. \quad (43)$$

Proof: See Appendix C. \square

In Theorem 3, we use an upper bound on the eavesdropper's rate, and consequently, obtain a lower bound on the ergodic secrecy rate. Therefore, maximizing the lower bound on the ergodic secrecy rate in (42) will yield a lower bound on the achievable ergodic secrecy rate, \bar{C}_{sec} , in (8).

Based on [32, Eq. (31)], the gradient of $R_{\text{eve},u}$ with respect to $\mathbf{P}_{s,\text{erg}}$ is given by

$$\nabla_{\mathbf{P}_{s,\text{erg}}} R_{\text{eve},u} = \frac{\log e}{M^{N_s} \sigma_e^2} \text{Diag} \left(\sum_{p_s=1}^{M^{N_s}} \frac{g_{p_s q_s} \mathbf{L}_{p_s q_s}^T}{\sum_{q_s=1}^{M^{N_s}} g_{p_s q_s}} \right) \quad (44)$$

where

$$g_{p_s q_s} = \exp \left(-\frac{\text{tr}(\mathbf{R}_{N_e}) \text{tr}(\mathbf{L}_{p_s q_s} \mathbf{P}_{s,\text{erg}})}{\sigma_e^2} \right) \quad (45)$$

$$\mathbf{L}_{p_s q_s} = \hat{\boldsymbol{\Sigma}}_s^2 \mathbf{V}_{s,\text{erg}} \mathbf{b}_{s,p_s,q_s} \mathbf{b}_{s,p_s,q_s}^H \mathbf{V}_{s,\text{erg}}^H. \quad (46)$$

The gradient of $R_{\text{eve},u}$ with respect to $\mathbf{V}_{s,\text{erg}}$ can be calculated as

$$\nabla_{\mathbf{V}_{s,\text{erg}}} R_{\text{eve},u} = \frac{\text{tr}(\mathbf{R}_{N_e}) \log e}{M^{N_s} \sigma_e^2} \sum_{p_s=1}^{M^{N_s}} \frac{1}{\sum_{q_s=1}^{M^{N_s}} g_{p_s q_s}} \sum_{q_s=1}^{M^{N_s}} g_{p_s q_s} \times \nabla_{\mathbf{V}_{s,\text{erg}}} \mathbf{b}_{s,p_s,q_s}^H \mathbf{V}_{s,\text{erg}}^H \mathbf{P}_{s,\text{erg}}^{\frac{1}{2}} \hat{\boldsymbol{\Sigma}}_s^2 \mathbf{P}_{s,\text{erg}}^{\frac{1}{2}} \mathbf{V}_{s,\text{erg}} \mathbf{b}_{s,p_s,q_s} \quad (47a)$$

$$= \frac{\text{tr}(\mathbf{R}_{N_e}) \log e}{M^{N_s} \sigma_e^2} \times \sum_{p_s=1}^{M^{N_s}} \frac{\sum_{q_s=1}^{M^{N_s}} g_{p_s q_s} \mathbf{P}_{s,\text{erg}}^{\frac{1}{2}} \hat{\boldsymbol{\Sigma}}_s^2 \mathbf{P}_{s,\text{erg}}^{\frac{1}{2}} \mathbf{V}_{s,\text{erg}} \mathbf{b}_{s,p_s,q_s} \mathbf{b}_{s,p_s,q_s}^H}{\sum_{q_s=1}^{M^{N_s}} g_{p_s q_s}}. \quad (47b)$$

Then, the gradients of $R_{\text{sec},1}(\mathbf{G})$ with respect to $\mathbf{P}_{s,\text{erg}}$ and $\mathbf{V}_{s,\text{erg}}$ are given by

$$\nabla_{\mathbf{P}_{s,\text{erg}}} \bar{R}_{\text{sec},1}(\mathbf{G}) = \nabla_{\mathbf{P}_{s,\text{erg}}} I(\mathbf{y}_{b,s,\text{erg}}; \mathbf{x}_{s,\text{erg}}) - \nabla_{\mathbf{P}_{s,\text{erg}}} R_{\text{eve},u} \quad (48)$$

$$\nabla_{\mathbf{V}_{s,\text{erg}}} \bar{R}_{\text{sec},1}(\mathbf{G}) = \nabla_{\mathbf{V}_{s,\text{erg}}} I(\mathbf{y}_{b,s,\text{erg}}; \mathbf{x}_{s,\text{erg}}) - \nabla_{\mathbf{V}_{s,\text{erg}}} R_{\text{eve},u} \quad (49)$$

where $\nabla_{\mathbf{P}_{s,\text{erg}}} I(\mathbf{y}_{b,s,\text{erg}}; \mathbf{x}_{s,\text{erg}})$ and $\nabla_{\mathbf{V}_{s,\text{erg}}} I(\mathbf{y}_{b,s,\text{erg}}; \mathbf{x}_{s,\text{erg}})$ are given in [43, Eq. (20)] and [43, Eq. (21)], respectively.

We propose Algorithm 2 to maximize the achievable ergodic secrecy rate $\bar{R}_{\text{sec},1}(\mathbf{G})$. It is important to note that the number of additions required for calculating $\bar{R}_{\text{sec},1}(\mathbf{G})$ in (42), $\nabla_{\mathbf{P}_{s,\text{erg}}} \bar{R}_{\text{sec},1}(\mathbf{G})$ in (48), and $\nabla_{\mathbf{V}_{s,\text{erg}}} \bar{R}_{\text{sec},1}(\mathbf{G})$ in (49) scales linearly with SM^{2N_s} . Therefore, for large N_t , the computational complexity of Algorithm 2 scales linearly with SM^{2N_s} . In contrast, the computational complexity of the secure transmission designs with statistical CSI in [1], [27] scales linearly with M^{2N_t} .

Define $N_3 = \text{rank}(\mathbf{T})$. Based on (43), we obtain the following theorem in the high SNR regime.

Theorem 4: If inequality $(k_{\text{erg}} - N_3)N_s \geq N_t$ holds, then we can always find a permutation $\{\ell_1, \dots, \ell_{N_t}\}$ for the PG-GSVD design in Theorem 3, which achieves $R_{\text{sec},1,\text{high}} = N_t \log_2 M b/s/Hz$ in the high SNR regime, i.e., the maximal secrecy rate is achieved. *Proof:* The proof follows similar steps as those in Appendix B if \mathbf{H}_{ea} is replaced by \mathbf{T} . \square

Remark 3: For small dimensional MIMO channels, $k_{\text{erg}} = N_3$ may hold. Thus, it is difficult to find a precoder design that achieves the maximal asymptotic secrecy rate when only

Algorithm 2: Maximizing $\bar{R}_{\text{sec},1}(\mathbf{G})$ with respect to $\mathbf{P}_{s,\text{erg}}$ and $\mathbf{V}_{s,\text{erg}}$.

- 1) Initialize $\mathbf{P}_{s,\text{erg}}$ and $\mathbf{V}_{s,\text{erg}}^{(0)}$ for $s = 1, \dots, S$ with $\text{tr}(\mathbf{A}_{\text{erg}} \mathbf{P}_{\text{erg}} \mathbf{A}_{\text{erg}}^H) = N_t$. Set N_{iter} and ε as the maximum number of iterations and a threshold, respectively.
- 2) Initialize $\bar{R}_{\text{sec},1}(\mathbf{G})$ based on (42). Set counter $n = 1$.
- 3) Update $\mathbf{P}_{s,\text{erg}}^{(n)}$ for $s = 1, \dots, S$ along the gradient decent direction $\nabla_{\mathbf{P}_{s,\text{erg}}} \bar{R}_{\text{sec},1}(\mathbf{G})$ based on (48).
- 4) Normalize $\mathbf{P}_{s,\text{erg}}^{(n)}$ to satisfy $\text{tr}(\mathbf{A}_{\text{erg}} \mathbf{P}_{\text{erg}} \mathbf{A}_{\text{erg}}^H) = N_t$.
- 5) Update $\mathbf{V}_{s,\text{erg}}^{(n)}$ for $s = 1, \dots, S$ along the gradient descent direction $\nabla_{\mathbf{V}_{s,\text{erg}}} \bar{R}_{\text{sec},1}(\mathbf{G})$ based on (49).
- 6) Compute $\bar{R}_{\text{sec},1}(\mathbf{G})^{(n+1)}$ based on (42). If $\bar{R}_{\text{sec},1}(\mathbf{G})^{(n+1)} - \bar{R}_{\text{sec},1}(\mathbf{G})^{(n)} > \varepsilon$ and $n \leq N_{\text{iter}}$, set $n = n + 1$ and repeat Steps 3–5;
- 7) Compute \mathbf{P}_{erg} and \mathbf{V}_{erg} based on $\mathbf{P}_{s,\text{erg}}^{(n)}$ and $\mathbf{V}_{s,\text{erg}}^{(n)}$.
Set $\mathbf{G}_{\text{erg}} = \mathbf{U}_{a,\text{erg}} \mathbf{A}_{\text{erg}} \mathbf{P}_{\text{erg}}^{\frac{1}{2}} \mathbf{V}_{\text{erg}}$.

statistical CSI of Eve is available at the transmitter. In this case, injection of AN may improve the secrecy rate in the high SNR regime, as shown in [1], [27]. On the other hand, for large-scale MIMO channels, it is known that typically $N_t > N_3$ holds [22], [33], [34]. Therefore, we have $k_{\text{erg}} - N_3 \neq 0$. By exploiting this property, we can formulate a PG-GSVD design similar to that in (69) and (70) to achieve the maximal secrecy rate in the high SNR regime by selecting a proper value for N_s . In this case, AN generation is not necessary in the high regime SNR.

B. AN Generation

As explained in Remark 3, for $(k_{\text{erg}} - N_3)N_s < N_t$, AN generation may be beneficial to increase the secrecy rate when the transmitter has only statistical CSI of Eve's channel. In particular, with perfect instantaneous CSI of Bob, the transmitter may construct the AN along the null space of \mathbf{H}_{ba} as follows [1], [27]:

$$\mathbf{x} = \mathbf{G}_{\text{erg},a} \mathbf{x}_a + \frac{\sqrt{P_{\text{AN}}}}{N_t - N_r} \mathbf{V}_b \mathbf{u} \quad (50)$$

where $\mathbf{G}_{\text{erg},a} \in \mathbb{C}^{N_t \times N_t}$ is the precoder for the useful signal, $\mathbf{V}_b \in \mathbb{C}^{N_t \times (N_t - N_r)}$ is the null space of \mathbf{H}_{ba} , and $\mathbf{u} \sim \mathcal{CN}(0, \mathbf{I}_{N_t - N_r})$ is the AN. After obtaining $\mathbf{G}_{\text{erg},a}$ via Algorithm 2, the AN power P_{AN} can be calculated as³ $P_{\text{AN}} = P - \text{tr} \{ \mathbf{G}_{\text{erg},a} \mathbf{G}_{\text{erg},a}^H \}$ [1], [27].

If Alice transmits AN, Eve's received signal is impaired by a zero-mean colored Gaussian noise vector with covariance matrix $P_{\text{AN}}/(N_t - N_r) \mathbf{H}_{ea} \mathbf{V}_b \mathbf{V}_b^H \mathbf{H}_{ea}^H + \sigma_e^2 \mathbf{I}_{N_e}$. For large-scale MIMO channels, as $N_t \rightarrow \infty$, we have

$$\mathbf{e}_i^H \mathbf{H}_{ea} \mathbf{V}_b \mathbf{V}_b^H \mathbf{H}_{ea}^H \mathbf{e}_j = \mathbf{e}_i^H \mathbf{R}_{N_e}^{\frac{1}{2}} \mathbf{H}_w \mathbf{R}_{N_t}^{\frac{1}{2}} \mathbf{V}_b \mathbf{V}_b^H \mathbf{R}_{N_t}^{\frac{1}{2}} \mathbf{H}_w^H \mathbf{R}_{N_e}^{\frac{1}{2}} \mathbf{e}_j \quad (51a)$$

³We note that although this power allocation policy and transmitting the AN in the null space of \mathbf{H}_{ea} are not optimal in general, simulations in [1], [27] show that such a design performs well when the transmitter has perfect statistical CSI of Eve's channel. A more general joint design of the precoder and the AN is provided in [28]. However, such a joint design has a significantly higher computational complexity when N_t is large. Therefore, for implementation simplicity, in this paper, we design the precoder and the AN separately as in [1], [27].

TABLE I: Number of additions required for calculating the mutual information and the MSE matrix for the system considered in Figure 1.

$4 \times 3 \times 2$	BPSK	QPSK
GSVD	8	16
Algorithm 1	32	512
Algorithm 1 in [1]	256	65536

TABLE II: Number of additions required for calculating the mutual information and the MSE matrix for the system considered in Figure 2.

$64 \times 48 \times 48$	BPSK	QPSK
GSVD	128	256
Algorithm 1	512	8192
Algorithm 1 in [1]	3.04e+038	1.15e+077

$$= \text{tr} \left(\mathbf{H}_w \mathbf{R}_{N_t}^{\frac{1}{2}} \mathbf{V}_b \mathbf{V}_b^H \mathbf{R}_{N_t}^{\frac{1}{2}} \mathbf{H}_w^H \mathbf{R}_{N_e}^{\frac{1}{2}} \mathbf{e}_j \mathbf{e}_i^H \mathbf{R}_{N_e}^{\frac{1}{2}} \right) \quad (51b)$$

$$\xrightarrow{N_t \rightarrow \infty} \text{tr}(\mathbf{R}_{N_t}^{\frac{1}{2}} \mathbf{V}_b \mathbf{V}_b^H \mathbf{R}_{N_t}^{\frac{1}{2}}) \text{tr} \left(\mathbf{R}_{N_e}^{\frac{1}{2}} \mathbf{e}_j \mathbf{e}_i^H \mathbf{R}_{N_e}^{\frac{1}{2}} \right) \quad (51c)$$

$$= \text{tr}(\mathbf{V}_b \mathbf{V}_b^H \mathbf{R}_{N_t}) \mathbf{e}_i^H \mathbf{R}_{N_e} \mathbf{e}_j \quad (51d)$$

where (51c) is based on [44, Eq. (102)]. As a result, we obtain

$$\frac{P_{\text{AN}}}{(N_t - N_r)} \mathbf{H}_{ea} \mathbf{V}_b \mathbf{V}_b^H \mathbf{H}_{ea}^H + \sigma_e^2 \mathbf{I}_{N_e} \xrightarrow{N_t \rightarrow \infty} \frac{P_{\text{AN}}}{(N_t - N_r)} \text{tr}(\mathbf{V}_b \mathbf{V}_b^H \mathbf{R}_{N_t}) \mathbf{R}_{N_e} + \sigma_e^2 \mathbf{I}_{N_e} = \mathbf{W}. \quad (52)$$

By whitening the noise with $\mathbf{W}^{-1/2}$ and following similar steps as in Appendix C, $R_{\text{eve},u}$ in (43) becomes

$$R_{\text{eve},u} = N_t \log M - \frac{1}{M^{N_s}} \sum_{s=1}^S \sum_{p_s=1}^{M^{N_s}} \log \sum_{q_s=1}^{M^{N_s}} \exp \left(-\text{tr}(\mathbf{R}_{N_e} \mathbf{W}^{-1}) \mathbf{b}_{s,p_s q_s}^H \mathbf{V}_{s,\text{erg}}^H \mathbf{P}_{s,\text{erg}}^{\frac{1}{2}} \hat{\Sigma}_s^2 \mathbf{P}_{s,\text{erg}}^{\frac{1}{2}} \mathbf{V}_{s,\text{erg}} \mathbf{b}_{s,p_s q_s} \right). \quad (53)$$

V. NUMERICAL RESULTS

We set $\sigma_b = \sigma_e$ and define $\text{SNR} = P/(N_r \sigma_b^2)$. Furthermore, we use $N_t \times N_r \times N_e$ to denote the simulated wiretap channel.

A. Scenarios with Instantaneous CSI of the Eavesdropper

In this subsection, the elements of \mathbf{H}_{ba} and \mathbf{H}_{ea} are generated independently and randomly. Tables I and II compare the computational complexities of the different schemes for the systems considered in Figures 1 and 2, respectively.

Figure 1 plots the secrecy rate for the $4 \times 3 \times 2$ wiretap channel for different precoder designs and different modulation schemes for $N_s = 2$. We observe from Figure 1 that Algorithm 1 achieves a similar performance as the precoder design in [1] but with orders of magnitude lower computational complexity as indicated in Table I. Both designs achieve the maximal rate $N_t \log_2 M$ b/s/Hz in the high SNR regime as indicated by Theorem 2. In contrast, the GSVD design yields an obvious rate loss in the high SNR regime. For the channels of Bob and Eve, we have $D_{b,1} = 0.57$ and $D_{e,1} = 0.81$, respectively. As explained in Example 1, the GSVD design sets

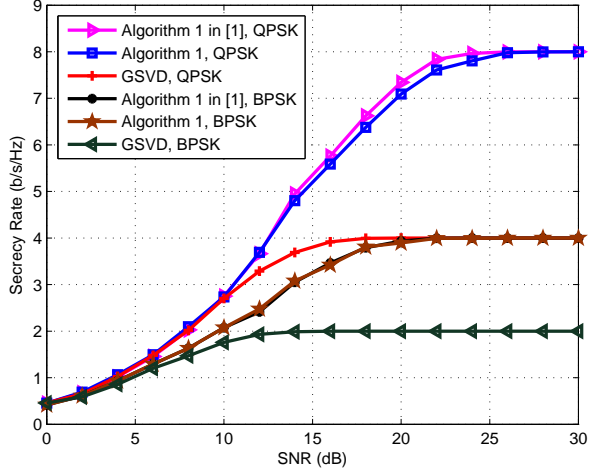


Fig. 1: Secrecy rate versus SNR for the $4 \times 3 \times 2$ wiretap channel for different precoder designs and different modulation schemes for $N_s = 2$.

$p_1 = p_2 = 0$ in this case. Therefore, the GSVD design suffers from a $2 \log_2 M$ b/s/Hz rate loss in the high SNR regime as shown in Figure 1.

In Figure 2, we show the secrecy rate for the $64 \times 48 \times 48$ wiretap channel for different precoder designs and different modulation schemes for $N_s = 2$. As indicated in Table II, the computational complexity of the precoder design in [1] is prohibitive in this case and no results can be shown. We observe that the secrecy rate of the GSVD design is lower than the upper bound given in Theorem 1. This is because for the GSVD design, as indicated in [26, Eq. (12)], only the non-zero subchannels of Bob which are stronger than the corresponding subchannels of Eve can be used for transmission. The b_i , $i = 1, \dots, s$, in (10) are in ascending order while the e_i , $i = 1, \dots, s$, in (11) are in descending order. Therefore, a large proportion of Bob's non-zero subchannels may be abandoned by the GSVD design for large-scale MIMO channels. As a result, Algorithm 1 achieves significantly higher secrecy rates than the GSVD design.

Figure 3 illustrates the convergence behavior of Algorithm 1 for different wiretap channels and different modulation schemes for $N_s = 2$ and SNR = 0 dB. Figure 3 shows the secrecy rate in each iteration. We observe that in all considered cases, Algorithm 1 converges within a few iterations.

Figure 4 plots the secrecy rate for Algorithm 1 for the $64 \times 48 \times 48$ wiretap channel for different modulation schemes and different N_s . For the $64 \times 48 \times 48$ wiretap channel, $k - N_2$ is equal to 16. As indicated by Theorem 2, when we set $N_s = 4$, Algorithm 1 can achieve the maximal rate $N_t \log_2 M$ b/s/Hz in the high SNR regime. This is validated in Figure 4.

B. Scenarios with Statistical CSI of the Eavesdropper

In Figure 5, we show the secrecy rate for Algorithm 2 for the $32 \times 32 \times 32$ wiretap channel for $N_s = 2$ and different modulation schemes. We set $\tilde{\mathbf{R}}_{N_b} = \mathbf{I}_{N_b}$ and $\mathbf{R}_{N_e} = \mathbf{I}_{N_e}$. Also, we generate $\tilde{\mathbf{R}}_{N_t}$ and \mathbf{R}_{N_t} based on [45, Eq. (3.14)],

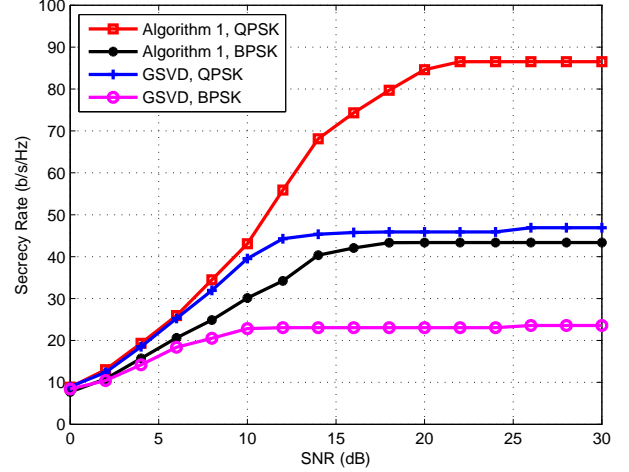


Fig. 2: Secrecy rate versus SNR for the $64 \times 48 \times 48$ wiretap channel for different precoder designs and different modulation schemes for $N_s = 2$.

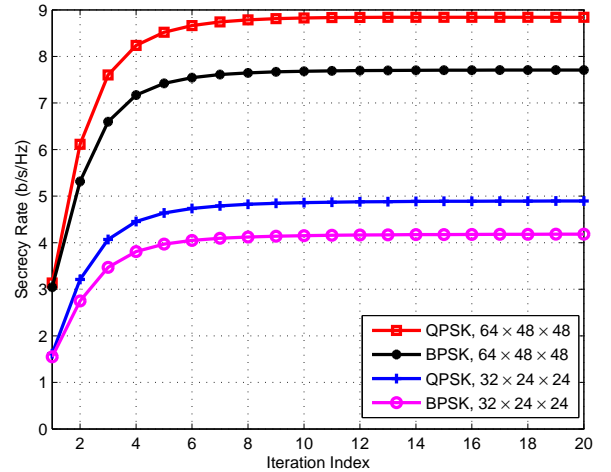


Fig. 3: Secrecy rate versus iteration index for different wiretap channels and different modulation schemes for Algorithm 1, $N_s = 2$, and SNR = 0 dB.

where the truncated Laplacian distribution is used to model the channel power angle spectrum [45]. The mean angle of arrival (AoA) is generated randomly and the AoA interval is $\mathcal{A} = [-\pi/6, \pi/6]$. The angular spread is set to be $\pi/2$. We generate one channel realization for the intended receiver's channel based on (6). Then, we evaluate the achievable ergodic secrecy rate based on (42). We observe that in the low-to-medium SNR regime, Algorithm 2 achieves nearly the same secrecy rate for all considered modulations. Furthermore, in the medium-to-high SNR regime, Algorithm 2 achieves a good secrecy rate performance for each modulation scheme.

Figure 6 and Figure 7 show the secrecy rate for Algorithm 2 for the $32 \times 24 \times 24$ wiretap channel for different modulation schemes, $N_s = 2$, and with/without artificial noise generation for urban and suburban scenarios, respectively.

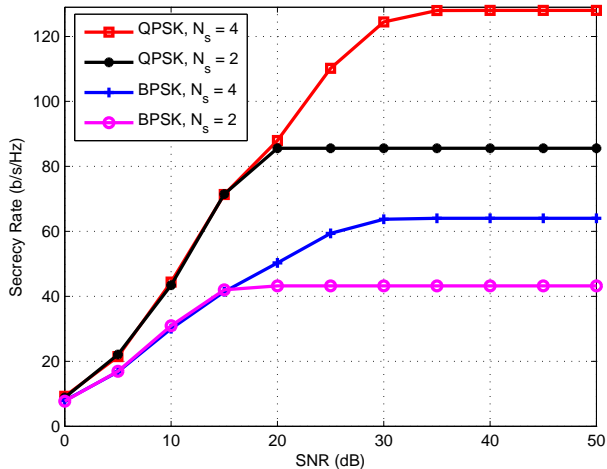


Fig. 4: Secrecy rate for Algorithm 1 versus SNR for the $64 \times 48 \times 48$ wiretap channel for different modulation schemes and different N_s .

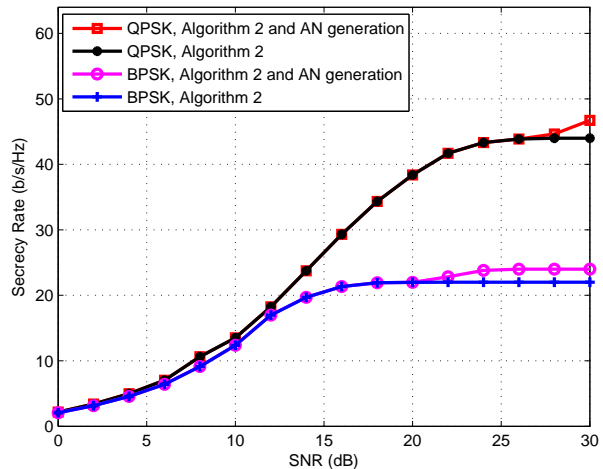


Fig. 6: Secrecy rate for Algorithm 2 versus SNR for the $32 \times 24 \times 24$ wiretap channel for different modulation schemes for $N_s = 2$, and an urban scenario.

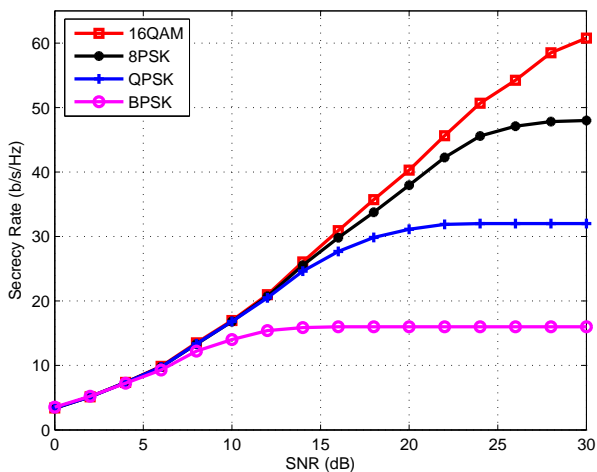


Fig. 5: Secrecy rate for Algorithm 2 versus SNR for the $32 \times 32 \times 32$ wiretap channel for different modulation schemes and $N_s = 2$.

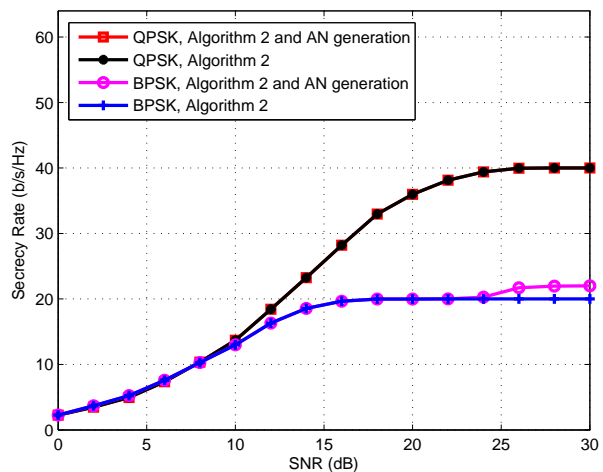


Fig. 7: Secrecy rate for Algorithm 2 versus SNR for the $32 \times 24 \times 24$ wiretap channel for different modulation schemes for $N_s = 2$ and a suburban scenario.

For these figures, we adopted the 3GPP SCM [46] for the urban scenario, half-wavelength antenna spacing at transmitter and receiver, respectively, a velocity of 36 km/h, and 6 paths. For the intended receiver's channel, we generate one channel realization based on the SCM model and use it in (9). For the eavesdropper's channel, we generate $L = 1000$ channel realizations \mathbf{H}_l , $l = 1, \dots, L$, based on the SCM model. According to the Kronecker fading MIMO channel model in (7), we can estimate $\mathbf{R}_{N_t} = \frac{1}{L} \sum_{l=1}^L \mathbf{H}_l^H \mathbf{H}_l$ and $\mathbf{R}_{N_e} = \frac{1}{L} \sum_{l=1}^L \mathbf{H}_l \mathbf{H}_l^H$ from these channel realizations. For the precoder design, we substitute the obtained \mathbf{R}_{N_t} and \mathbf{R}_{N_e} into the achievable ergodic secrecy rate expression in (42). Figure 6 and Figure 7 indicate that Algorithm 2 achieves good secrecy rate performance for both urban and suburban scenarios. Also, AN generation is beneficial and achieves a

secrecy rate gain in the high SNR regime.

We note that in the low SNR regime, Proposition 2 in [1] proves that the optimal transmission policy for MIMO wiretap channels with finite alphabet inputs is beamforming. Therefore, in the low SNR regime, the optimal performance of the complete search design in [1] and the proposed low complexity design should be the same since only one sub-channel is used for transmission regardless of the value of N_s . Moreover, it is also proved in [1] that for low SNR the optimal secrecy rate is independent of the constellation size. Therefore, as indicated in Figure 5, in the low-to-moderate SNR regime, the secrecy rates of the proposed low complexity precoder are virtually the same for QPSK, 8PSK, and 16QAM modulations. In the high SNR regime, Theorem 3 in this paper indicates that as long as $(k - N_2)N_s \neq N_t$ holds, we can

always find a low complexity precoder design to achieve the saturation secrecy rate regardless of the constellation size. In the moderate-to-high SNR regime, we expect the performance gap between the proposed low complexity design and the complete search design in [1] to increase to some extent with the constellation size. However, we note that even for the case of $N_t = 4$, cf. Table I, it will be difficult to simulate the complete search design in [1] for 16QAM modulation since the computational complexity scales linearly with 16^8 for each iteration in Algorithm 1 in [1]. However, the proposed low complexity precoder design can be efficiently implemented even for the case of $N_t = 32$ and 16QAM modulation, as shown in Figure 5.

VI. CONCLUSION

In this paper, we have investigated the linear precoder design for large-scale MIMOME wiretap channels with finite alphabet inputs. For the case where the transmitter has instantaneous CSI of the eavesdropper, we derived an upper bound on the secrecy rate for the GSVD design in the high SNR regime. The derived expression reveals that the GSVD design may lead to a serious performance loss. Motivated by this, we proposed a novel PG-GSVD design to overcome the negative properties of the GSVD design while retaining its low computational complexity for large-scale MIMO systems. We further extended the PG-GSVD design to the case where only statistical CSI of the eavesdropper is available at the transmitter. For massive MIMO channels with strong transmit correlation, we proved that the proposed PG-GSVD design with statistical CSI of the eavesdropper can achieve the maximal secrecy rate for finite alphabet inputs for the MIMOME wiretap channel in the high SNR regime. For massive MIMO channels with weak transmit correlation, we proposed an AN generation scheme to improve the secrecy rate in the high SNR regime. Simulation results indicated that the proposed designs perform well in large-scale MIMOME wiretap channels and achieve substantial secrecy rate gains compared to the GSVD design for finite alphabet inputs while requiring a substantially lower computational complexity compared to the existing precoder design in [1]. Possible extensions of the proposed designs include the consideration of imperfect CSI of the intended user channel, multiuser settings, and the multi-cell scenarios with pilot contamination.

APPENDIX A PROOF OF THEOREM 1

Based on (10) and (16), $I(\mathbf{y}_b; \mathbf{x}_a)$ in (5) for the GSVD design becomes

$$I(\mathbf{y}_b; \mathbf{x}_a) = \sum_{i=1}^s I(b_i^2 p_{k-r-s+i}) + \sum_{i=1}^r I(p_{k-s+i}) \quad (54)$$

where $I(\gamma) = I(x; \sqrt{\gamma}x + n)$. Therefore, for $P \rightarrow \infty$, we obtain

$$\lim_{P \rightarrow \infty} I(\mathbf{y}_b; \mathbf{x}_a) \leq (s+r) \log_2(M). \quad (55)$$

According to Inclusion–Exclusion Principle [47], we know

$$\dim(\mathcal{S}_{ba}) + \dim(\mathcal{S}_{be}) = \dim(\mathcal{S}_{ba} \cup \mathcal{S}_{be}) - \dim(\mathcal{S}_{ba} \cap \mathcal{S}_{be}). \quad (56)$$

For the subspaces \mathcal{S}_{ba} and \mathcal{S}_{be} , we have

$$\begin{aligned} & \mathcal{S}_{ba} \cap \mathcal{S}_{be} \\ &= \left(\text{null}(\mathbf{H}_{ba})^\perp \cap \text{null}(\mathbf{H}_{ea}) \right) \cap \left(\text{null}(\mathbf{H}_{ba})^\perp \cap \text{null}(\mathbf{H}_{ea})^\perp \right) \end{aligned} \quad (57a)$$

$$= \left(\text{null}(\mathbf{H}_{ba})^\perp \cap \text{null}(\mathbf{H}_{ea}) \right) \cap \left(\text{null}(\mathbf{H}_{ea})^\perp \cap \text{null}(\mathbf{H}_{ba})^\perp \right) \quad (57b)$$

$$= \text{null}(\mathbf{H}_{ba})^\perp \cap \left(\left(\text{null}(\mathbf{H}_{ea}) \right) \cap \text{null}(\mathbf{H}_{ea})^\perp \right) \cap \text{null}(\mathbf{H}_{ba})^\perp \quad (57c)$$

$$= \emptyset \quad (57d)$$

where (57b) and (57c) are obtained based on the properties of intersections [48].

Also, we have

$$\begin{aligned} & \mathcal{S}_{ba} \cup \mathcal{S}_{be} \\ &= \left(\text{null}(\mathbf{H}_{ba})^\perp \cap \text{null}(\mathbf{H}_{ea}) \right) \cup \left(\text{null}(\mathbf{H}_{ba})^\perp \cap \text{null}(\mathbf{H}_{ea})^\perp \right) \end{aligned} \quad (58a)$$

$$= \text{null}(\mathbf{H}_{ba})^\perp \cap \left(\text{null}(\mathbf{H}_{ea}) \cup \text{null}(\mathbf{H}_{ea})^\perp \right) \quad (58b)$$

$$= \text{null}(\mathbf{H}_{ba})^\perp \quad (58c)$$

where (58b) and (58c) are obtained based on the Distributive Law of sets [48] and the Rank–Nullity Theorem [49], respectively.

From (56)–(58), we obtain

$$s + r = \dim(\mathcal{S}_{ba}) + \dim(\mathcal{S}_{be}) = \dim\left(\text{null}(\mathbf{H}_{ba})^\perp\right). \quad (59)$$

Assuming $\mathbf{v}_i \in \mathbb{C}^{N_t \times 1}$ and $\mathbf{u}_j \in \mathbb{C}^{N_r \times 1}$ are the N_t left and N_r right singular vectors of \mathbf{H}_{ba} , respectively, $i = 1, \dots, N_t$, $j = 1, \dots, N_r$, \mathbf{H}_{ba} can be written as

$$\mathbf{H}_{ba} = \sum_{i=1}^{N_1} \lambda_i \mathbf{u}_i \mathbf{v}_i^H \quad (60)$$

where λ_i is the singular value of \mathbf{H}_{ba} . For $N_1 < N_t$, we have

$$\text{null}(\mathbf{H}_{ba}) = \sum_{i=N_1+1}^{N_t} \omega_i \mathbf{v}_i \mathbf{v}_i^H \quad (61)$$

where ω_i denotes an arbitrary non-zero complex value, $i = 1, \dots, N_t$. Based on the property of the orthogonal complement of a subspace [50], we obtain

$$\left(\text{null}(\mathbf{H}_{ba})^\perp \right) = \left(\sum_{i=N_1+1}^{N_t} \omega_i \mathbf{v}_i \mathbf{v}_i^H \right)^\perp \quad (62a)$$

$$= \text{null} \left(\sum_{i=N_1+1}^{N_t} \omega_i \mathbf{v}_i \mathbf{v}_i^H \right) \quad (62b)$$

$$= \sum_{i=1}^{N_1} \omega_i \mathbf{v}_i \mathbf{v}_i^H. \quad (62c)$$

Therefore, we have

$$\dim\left(\text{null}(\mathbf{H}_{ba})^\perp\right) = N_1. \quad (63)$$

For $N_1 = N_t$, $\text{null}(\mathbf{H}_{ba}) = \emptyset$, and we obtain

$$\dim\left(\text{null}(\mathbf{H}_{ba})^\perp\right) = N_t. \quad (64)$$

Combining (5), (55), (59), (63), and (64) completes the proof.

APPENDIX B
PROOF OF THEOREM 2

The key idea of achieving the maximal rate $N_t \log M$ b/s/Hz in the high SNR regime is to guarantee that all N_t signals can be received by Bob but not by Eve. To achieve this, N_s signals are combined into a group and transmitted along the subchannels \mathbf{R}_r in (20). As a result, we need to analyze the dimension of \mathcal{S}_{ba} .

Based on the Inclusion–Exclusion Principle [47], we have $\dim(\mathcal{S}_{ba}) + \dim(\mathcal{S}_n) = \dim(\mathcal{S}_{ba} \cup \mathcal{S}_n) - \dim(\mathcal{S}_{ba} \cap \mathcal{S}_n)$. (65)

Following similar steps as in (57) and (58), we obtain

$$\mathcal{S}_{ba} \cap \mathcal{S}_n = \left(\text{null}(\mathbf{H}_{ba})^\perp \cap \text{null}(\mathbf{H}_{ea}) \right) \cap \left(\text{null}(\mathbf{H}_{ba}) \cap \text{null}(\mathbf{H}_{ea}) \right) \quad (66a)$$

$$= \left(\text{null}(\mathbf{H}_{ea}) \cap \text{null}(\mathbf{H}_{ba})^\perp \right) \cap \left(\text{null}(\mathbf{H}_{ba}) \cap \text{null}(\mathbf{H}_{ea}) \right) \quad (66b)$$

$$= \text{null}(\mathbf{H}_{ea}) \cap \left(\text{null}(\mathbf{H}_{ba})^\perp \cap \text{null}(\mathbf{H}_{ba}) \right) \cap \text{null}(\mathbf{H}_{ea}) \quad (66c)$$

$$= \emptyset \quad (66d)$$

and

$$\mathcal{S}_{ba} \cup \mathcal{S}_n = \left(\text{null}(\mathbf{H}_{ba})^\perp \cap \text{null}(\mathbf{H}_{ea}) \right) \cup \left(\text{null}(\mathbf{H}_{ba}) \cap \text{null}(\mathbf{H}_{ea}) \right) \quad (67a)$$

$$= \text{null}(\mathbf{H}_{ea}) \cap \left(\text{null}(\mathbf{H}_{ba})^\perp \cup \text{null}(\mathbf{H}_{ba}) \right) \quad (67b)$$

$$= \text{null}(\mathbf{H}_{ea}). \quad (67c)$$

Since $\text{rank}(\mathbf{H}_{ea}) = N_2$, we have $\dim(\text{null}(\mathbf{H}_{ea})) = N_t - N_2$. Then, based on (65), (66d), (67c), we obtain

$$r + N_t - k = N_t - N_2. \quad (68)$$

From (68), we know $r = k - N_2$.

When $(k - N_2)N_s \geq N_t$, we design the PG-GSVD precoder in (24) as follows. We set

$$\mathbf{P} = \begin{matrix} & k-r-s & s & r & N_t-k \\ \begin{matrix} k-r-s \\ s \\ r \\ N_t-k \end{matrix} & \begin{bmatrix} \mathbf{0} & \mathbf{0} & \mathbf{0} & \mathbf{0} \\ \mathbf{0} & \mathbf{0} & \mathbf{0} & \mathbf{0} \\ \mathbf{0} & \mathbf{0} & \text{diag}(p_1, \dots, p_r) & \mathbf{0} \\ \mathbf{0} & \mathbf{0} & \mathbf{0} & \mathbf{0} \end{bmatrix} & \end{matrix} \cdot \quad (69)$$

Also, we select a pairing scheme $\{\ell_1, \dots, \ell_{N_t}\}$ in (25) satisfying

$$[\mathbf{P}_s]_{ii} = \begin{cases} 0 & \text{if } 1 \leq i \leq N_s - 1 \\ \frac{p_j}{\omega_{k-r+j}} & \text{if } i = N_s \end{cases} \quad (70)$$

for $s = 1, \dots, S$, $i = 1, \dots, N_s$, and $j = 1, \dots, r$.

Based on the design in (69) and (70), in the high SNR regime, we have

$$I(\mathbf{y}_{b,s}; \mathbf{x}_s) \xrightarrow{P \rightarrow \infty} N_s \log M \quad (71)$$

$$I(\mathbf{y}_{e,s}; \mathbf{x}_s) = 0. \quad (72)$$

Substituting (71) and (72) into (31) completes the proof.

APPENDIX C
PROOF OF THEOREM 3

By setting $\mathbf{G}_{\text{erg}} = \mathbf{U}_{a,\text{erg}} \mathbf{A}_{\text{erg}} \mathbf{P}_{\text{erg}}^{\frac{1}{2}} \mathbf{V}_{\text{erg}}$, we know $I(\mathbf{y}_b; \mathbf{x}_a)$ in (9) can be written as

$$I(\mathbf{y}_b; \mathbf{x}_a) = \sum_{s=1}^S I(\mathbf{y}_{b,s,\text{erg}}; \mathbf{x}_{s,\text{erg}}). \quad (73)$$

Next, we consider $E[I(\mathbf{y}_e; \mathbf{x}_a)]$. In the expression of $I(\mathbf{y}_e; \mathbf{x}_a)$ in [1, Eq. (12)], $\log \exp(\sum x_k)$ is a convex function. Therefore, by applying Jensen's inequality to $I(\mathbf{y}_e; \mathbf{x}_a)$, we obtain an upper bound on $E[I(\mathbf{y}_e; \mathbf{x}_a)]$

$$E[I(\mathbf{y}_e; \mathbf{x}_a)] \leq R_{\text{eve,u}} = N_t \log M - \frac{1}{M^{N_t}} \sum_{p=1}^{M^{N_t}} \log \sum_{q=1}^{M^{N_t}} \exp \left(-\frac{\text{tr}(\mathbf{R}_{N_e})}{\sigma_e^2} \mathbf{b}_{pq}^H \mathbf{G}^H \mathbf{R}_{N_t} \mathbf{G} \mathbf{b}_{pq} \right) \quad (74)$$

Substituting $\mathbf{G} = \mathbf{G}_{\text{erg}}$, $\mathbf{R}_{N_t} = \mathbf{T}^H \mathbf{T}$, and (39) in (74), we have

$$R_{\text{eve,u}} = N_t \log M - \frac{1}{M^{N_t}} \sum_{p=1}^{M^{N_t}} \log \sum_{q=1}^{M^{N_t}} \exp \left(-\frac{\text{tr}(\mathbf{R}_{N_e})}{\sigma_e^2} \mathbf{b}_{pq}^H \mathbf{V}_{\text{erg}}^H \mathbf{P}_{\text{erg}}^{\frac{1}{2}} \tilde{\Sigma}_{ea,\text{erg}}^2 \mathbf{P}_{\text{erg}}^{\frac{1}{2}} \mathbf{V}_{\text{erg}} \mathbf{b}_{pq} \right). \quad (75)$$

Considering the structure of \mathbf{P}_{erg} and \mathbf{V}_{erg} in Section IV-A, $R_{\text{eve,u}}$ can be further simplified as in (76a)–(76f) at the top of the next page.

Combining (9), (73), (74), and (76f) completes the proof.

REFERENCES

- [1] Y. Wu, C. Xiao, Z. Ding, X. Gao, and S. Jin, "Linear precoding for finite-alphabet signaling over MIMOME wiretap channels," *IEEE Trans. Veh. Technol.*, vol. 61, pp. 2599–2612, Jul. 2012.
- [2] N. Yang, L. Wang, G. Geraci, M. Elkashlan, J. Yuan, and M. D. Renzo, "Safeguarding 5G wireless communication networks using physical layer security," *IEEE Commun. Magazine*, vol. 53, pp. 20–27, Apr. 2015.
- [3] A. D. Wyner, "The wiretap channel," *Bell Syst. Tech. J.*, vol. 54, pp. 1355–1387, Oct. 1975.
- [4] S. Shafiee and S. Ulukus, "Achievable rates in Gaussian MISO channels with secrecy constraints," in *Proc. IEEE Int. Symp. Inf. Theory (ISIT'2007)*, Nice, France, Jun. 2007, pp. 2466–2470.
- [5] E. Tekin and A. Yener, "The general Gaussian multiple-access and two-way wiretap channels: Achievable rates and cooperative jamming," *IEEE Trans. Inf. Theory*, vol. 54, pp. 2735–2751, Jun. 2008.
- [6] A. Khisti and G. W. Wornell, "Secure transmission with multiple antennas-Part I: The MISOME wiretap channel," *IEEE Trans. Inf. Theory*, vol. 56, pp. 3088–3104, Jul. 2010.
- [7] —, "Secure transmission with multiple antennas-Part II: The MIMOME wiretap channel," *IEEE Trans. Inf. Theory*, vol. 56, pp. 5515–5532, Nov. 2010.
- [8] J. Li and A. P. Petropulu, "On ergodic secrecy rate for Gaussian MISO wiretap channel," *IEEE Trans. Wireless Commun.*, vol. 10, pp. 1176–1187, Apr. 2011.
- [9] M. C. Gursoy, "Secure communication in the low-SNR regime," *IEEE Trans. Commun.*, vol. 60, pp. 1114–1123, Apr. 2012.
- [10] L. Liu, R. Zhang, and K.-C. Chua, "Secrecy wireless information and power transfer with MISO beamforming," *IEEE Trans. Signal Process.*, vol. 62, pp. 1850–1863, Apr. 2014.
- [11] Z. Rezki, A. Khisti, and M.-S. Alouini, "On ergodic secrecy rate for Gaussian MISO wiretap channel," *IEEE Trans. Wireless Commun.*, vol. 13, pp. 3364–3379, Jun. 2014.

$$R_{\text{eve, u}} = N_t \log M - \frac{1}{M^{N_t}} \sum_{p=1}^{M^{N_t}} \log \sum_{q=1}^{M^{N_t}} \exp \left(-\frac{\text{tr}(\mathbf{R}_{N_e})}{\sigma_e^2} \sum_{s=1}^S \mathbf{b}_{s,pq}^H \mathbf{V}_{s,\text{erg}}^H \mathbf{P}_{s,\text{erg}}^{\frac{1}{2}} \hat{\Sigma}_s^2 \mathbf{P}_{s,\text{erg}}^{\frac{1}{2}} \mathbf{V}_{s,\text{erg}} \mathbf{b}_{s,pq} \right) \quad (76a)$$

$$= N_t \log M - \frac{1}{M^{N_t}} \sum_{p=1}^{M^{N_t}} \log \sum_{q=1}^{M^{N_t}} \prod_{s=1}^S \exp \left(-\frac{\text{tr}(\mathbf{R}_{N_e})}{\sigma_e^2} \mathbf{b}_{s,pq}^H \mathbf{V}_{s,\text{erg}}^H \mathbf{P}_{s,\text{erg}}^{\frac{1}{2}} \hat{\Sigma}_s^2 \mathbf{P}_{s,\text{erg}}^{\frac{1}{2}} \mathbf{V}_{s,\text{erg}} \mathbf{b}_{s,pq} \right) \quad (76b)$$

$$= N_t \log M - \frac{1}{M^{N_t}} \sum_{p=1}^{M^{N_t}} \log \sum_{q_1=1}^{M^{N_s}} \cdots \sum_{q_S=1}^{M^{N_s}} \prod_{s=1}^S \exp \left(-\frac{\text{tr}(\mathbf{R}_{N_e})}{\sigma_e^2} \mathbf{b}_{s,pq_s}^H \mathbf{V}_{s,\text{erg}}^H \mathbf{P}_{s,\text{erg}}^{\frac{1}{2}} \hat{\Sigma}_s^2 \mathbf{P}_{s,\text{erg}}^{\frac{1}{2}} \mathbf{V}_{s,\text{erg}} \mathbf{b}_{s,pq_s} \right) \quad (76c)$$

$$= N_t \log M - \frac{1}{M^{N_t}} \sum_{p=1}^{M^{N_t}} \log \sum_{q_1=1}^{M^{N_s}} \exp \left(-\frac{\text{tr}(\mathbf{R}_{N_e})}{\sigma_e^2} \mathbf{b}_{1,pq_1}^H \mathbf{V}_{1,\text{erg}}^H \mathbf{P}_{1,\text{erg}}^{\frac{1}{2}} \hat{\Sigma}_1^2 \mathbf{P}_{1,\text{erg}}^{\frac{1}{2}} \mathbf{V}_{1,\text{erg}} \mathbf{b}_{1,pq_1} \right) \quad (76d)$$

$$\times \cdots \times \sum_{q_S=1}^{M^{N_s}} \exp \left(-\frac{\text{tr}(\mathbf{R}_{N_e})}{\sigma_e^2} \mathbf{b}_{S,pq_S}^H \mathbf{V}_{S,\text{erg}}^H \mathbf{P}_{S,\text{erg}}^{\frac{1}{2}} \hat{\Sigma}_S^2 \mathbf{P}_{S,\text{erg}}^{\frac{1}{2}} \mathbf{V}_{S,\text{erg}} \mathbf{b}_{S,pq_S} \right)$$

$$= N_t \log M - \frac{1}{M^{N_t}} \sum_{p=1}^{M^{N_t}} \sum_{s=1}^S \log \sum_{q_s=1}^{M^{N_s}} \exp \left(-\frac{\text{tr}(\mathbf{R}_{N_e})}{\sigma_e^2} \mathbf{b}_{s,pq_s}^H \mathbf{V}_{s,\text{erg}}^H \mathbf{P}_{s,\text{erg}}^{\frac{1}{2}} \hat{\Sigma}_s^2 \mathbf{P}_{s,\text{erg}}^{\frac{1}{2}} \mathbf{V}_{s,\text{erg}} \mathbf{b}_{s,pq_s} \right) \quad (76e)$$

$$= N_t \log M - \frac{1}{M^{N_t}} \sum_{s=1}^S \sum_{p_s=1}^{M^{N_s}} \log \sum_{q_s=1}^{M^{N_s}} \exp \left(-\frac{\text{tr}(\mathbf{R}_{N_e})}{\sigma_e^2} \mathbf{b}_{s,p_s q_s}^H \mathbf{V}_{s,\text{erg}}^H \mathbf{P}_{s,\text{erg}}^{\frac{1}{2}} \hat{\Sigma}_s^2 \mathbf{P}_{s,\text{erg}}^{\frac{1}{2}} \mathbf{V}_{s,\text{erg}} \mathbf{b}_{s,p_s q_s} \right). \quad (76f)$$

- [12] J. Zhu, R. Schober, and V. K. Bhargava, "Secure transmission in multi-cell massive MIMO systems," *IEEE Trans. Wireless Commun.*, vol. 13, pp. 4766–4781, Sep. 2014.
- [13] F. Zhu, F. Gao, M. Yao, and H. Zou, "Joint information and jamming beamforming for physical layer security with full duplex base station," *IEEE Trans. Signal Process.*, vol. 62, pp. 6391–6401, Dec. 2014.
- [14] L. Wang, S. Bashar, Y. Wei, and R. Li, "Secrecy enhancement analysis against unknown eavesdropping in spatial modulation," *IEEE Commun. Lett.*, vol. 19, pp. 1351–1354, Aug. 2015.
- [15] X. Chen, C. Zhong, C. Yuen, and H.-H. Chen, "Multi-antenna relay aided wireless physical layer security," *IEEE Commun. Mag.*, vol. 53, pp. 40–46, Dec. 2015.
- [16] X. Chen, L. Lei, H. Zhang, and C. Yuen, "Large-scale MIMO relaying techniques for physical layer security: AF or DF?" *IEEE Trans. Wireless Commun.*, vol. 14, pp. 5135–5146, Sep. 2015.
- [17] F. Zhu, F. Gao, T. Zhang, K. Sun, and M. Yao, "Physical-layer security for full duplex communications with self-interference mitigation," *IEEE Trans. Wireless Commun.*, vol. 15, pp. 329–340, Jan. 2016.
- [18] J. Zhu, R. Schober, and V. K. Bhargava, "Linear precoding of data and artificial noise in secure massive MIMO systems," *IEEE Trans. Wireless Commun.*, vol. 15, pp. 2245–2261, Mar. 2016.
- [19] L. Wang, R. Li, C. Cao, and G. L. Stüber, "SNR analysis of time reversal signaling on target and unintended receivers in distributed transmission," *IEEE Trans. Commun.*, vol. 64, pp. 2176–2191, May 2016.
- [20] H.-M. Wang, C. Wang, and D. W. K. Ng, "Artificial noise assisted secure transmission under training and feedback," *IEEE Trans. Signal Process.*, vol. 63, pp. 6285–6298, Dec. 2015.
- [21] W. Zeng, Y. R. Zheng, and C. Xiao, "Multi-antenna secure cognitive radio networks with finite-alphabet inputs: A global optimization approach for precoder design," *IEEE Trans. Wireless Commun.*, vol. 15, pp. 3044–3057, Apr. 2016.
- [22] Y. Wu, R. Schober, D. W. K. Ng, C. Xiao, and G. Caire, "Secure massive MIMO transmission with an active eavesdropper," *IEEE Trans. Inf. Theory*, vol. 62, pp. 3880–3900, Jul. 2016.
- [23] H.-M. Wang, C. Wang, D. W. K. Ng, M. H. Lee, and J. Xiao, "Artificial noise-assisted secure transmission for distributed antenna systems," *IEEE Trans. Signal Process.*, vol. 64, pp. 4050–4064, Aug. 2016.
- [24] Y. Zou, J. Zhu, X. Wang, and L. Hanzo, "A survey on wireless security: Technical challenges, recent advances and future trends," *Proceedings of the IEEE*, vol. 104, pp. 1727–1765, Sep. 2016.
- [25] Y. Zou, "Physical-layer security for spectrum sharing systems," *IEEE Trans. Wireless Commun.*, vol. 16, pp. 1319–1329, Feb. 2017.
- [26] S. Bashar, Z. Ding, and C. Xiao, "On secrecy rate analysis of MIMO wiretap channels driven by finite-alphabet input," *IEEE Trans. Commun.*, vol. 60, pp. 3816–3825, Dec. 2012.
- [27] —, "On the secrecy rate of multi-antenna wiretap channel under finite-alphabet input," *IEEE Commun. Lett.*, vol. 15, pp. 527–529, May 2011.
- [28] S. R. Aghdam and T. M. Duman, "Low complexity precoding for MIMOME wiretap channels based on cut-off rate," in *Proc. IEEE Int. Symp. Inf. Theory (ISIT'2016)*, Barcelona, Spain, Jul. 2016, pp. 2988–2992.
- [29] A. Lozano, A. M. Tulino, and S. Verdú, "Optimum power allocation for parallel Gaussian channels with arbitrary input distributions," *IEEE Trans. Inform. Theory*, pp. 3033–3051, Jul. 2006.
- [30] Y. Wu, M. Wang, C. Xiao, Z. Ding, and X. Gao, "Linear precoding for MIMO broadcast channels with finite-alphabet constraints," *IEEE Trans. Wireless Commun.*, vol. 11, pp. 2906–2920, Aug. 2012.
- [31] Y. Wu, C. Xiao, X. Gao, J. D. Matyjas, and Z. Ding, "Linear precoder design for MIMO interference channels with finite-alphabet signaling," *IEEE Trans. Commun.*, vol. 61, pp. 3766–3780, Sep. 2013.
- [32] C. Xiao, Y. R. Zheng, and Z. Ding, "Globally optimal linear precoders for finite alphabet signals over complex vector Gaussian channels," *IEEE Trans. Signal Process.*, pp. 3301–3314, Jul. 2011.
- [33] A. Adhikary, J. Nam, J.-Y. Ahn, and G. Caire, "Joint spatial division and multiplexing—The large-scale array regime," *IEEE Trans. Inf. Theory*, vol. 59, pp. 6441–6463, Oct. 2013.
- [34] H. Yin, D. Gesbert, and L. Cottarelli, "Dealing with interference in distributed large-scale MIMO systems: A statistical approach," *IEEE J. Sel. Topics Signal Process.*, vol. 8, pp. 942–953, Oct. 2014.
- [35] T. L. Marzetta, "Noncooperative cellular wireless with unlimited numbers of base station antennas," *IEEE Trans. Wireless Commun.*, vol. 15, pp. 3590–3600, Nov. 2010.
- [36] E. G. Larsson, O. Edfors, F. Tufvesson, and T. L. Marzetta, "Massive MIMO for next generation wireless systems," *IEEE Commun. Mag.*, vol. 52, pp. 186–195, Feb. 2014.
- [37] S. K. Mohammed, E. Viterbo, Y. Hong, and A. Chockalingam, "Precoding by pairing subchannels to increase MIMO capacity with discrete input alphabets," *IEEE Trans. Inform. Theory*, pp. 4156–4169, Jul. 2011.
- [38] T. Ketseoglou and E. Ayanoglu, "Linear precoding for MIMO with LDPC coding and reduced complexity," *IEEE Trans. Wireless Commun.*, pp. 2192–2204, Apr. 2015.
- [39] Y. Wu, D. W. K. Ng, C. W. Wen, R. Schober, and A. Lozano, "Low-complexity MIMO precoding with discrete signals and statistical CSI," in *Proc. IEEE Int. Telecommun. Conf. (ICC'2016)*, Kuala Lumpur, Malaysia, May 2016, pp. 1–6.

- [40] D. P. Palomar and S. Verdú, "Gradient of mutual information in linear vector Gaussian channels," *IEEE Trans. Inform. Theory*, vol. 52, pp. 141–154, Jan. 2006.
- [41] W. Zeng, C. Xiao, M. Wang, and J. Lu, "Linear precoding for finite-alphabet inputs over MIMO fading channels with statistical CSI," *IEEE Trans. Signal Process.*, pp. 3134–3148, Jun. 2012.
- [42] F. Pérez-Cruz, M. R. D. Rodrigues, and S. Verdú, "MIMO Gaussian channels with arbitrary inputs: Optimal precoding and power allocation," *IEEE Trans. Inform. Theory*, vol. 56, pp. 1070–1084, Mar. 2010.
- [43] Y. Wu, C.-K. Wen, C. Xiao, X. Gao, and R. Schober, "Linear precoding for the MIMO multiple access channel with finite alphabet inputs and statistical CSI," *IEEE Trans. Wireless Commun.*, vol. 14, pp. 983–997, Feb. 2015.
- [44] C.-K. Wen, G. Pan, K.-K. Wong, M. Guo, and J.-C. Chen, "A deterministic equivalent for the analysis of non-Gaussian correlated MIMO multiple access channels," *IEEE Trans. Inf. Theory*, vol. 59, pp. 329–352, Jan. 2013.
- [45] Y. S. Cho, J. Kim, W. Y. Yang, and C. G. Kang, *MIMO-OFDM Wireless Communications with MATLAB*. Singapore: John Wiley & Sons (Asia) Pte Ltd, 2010.
- [46] J. Salo, G. Del Galdo, J. Salmi, P. Kyösti, M. Milojevic, D. Lasselva, and C. Schneider, (2005, Jan.) MATLAB implementation of the 3GPP Spatial Channel Model (3GPP TR 25.996), [Online]. Available: <http://www.tkk.fi/Units/Radio/scm/>.
- [47] G. E. Andrews, *Number Theory*. Philadelphia, PA: Saunders, 1971.
- [48] R. P. Halmos, *Naive Set Theory*. New Jersey: Van Nostrand, 1960.
- [49] S. Banerjee and A. Roy, *Linear Algebra and Matrix Analysis for Statistics*. London: Chapman and Hall/CRC, 2014.
- [50] R. P. Halmos, *Finite-dimensional vector spaces*. New York: Springer-Verlag, 1974.